# u S

University of
Stavanger

**Faculty of Science and Technology**

# MASTER'S THESIS

| Study program/ Specialization:<br><br>**Offshore Technology / Subsea Technology** | Spring semester, 2016<br><br>Open / ~~Restricted access~~ |
|---|---|
| Writer:<br>**Utari Cendhy Liestyarini** | ……………………… |

Faculty supervisor: **Prof. Muk Chen Ong**

External supervisor: **Dr. Yihan Xing (ROXAR, Emerson Process Management)**

Thesis title:

**CFD Analysis of Internal Pipe Flows**

Credits (ECTS): **30**

| Key words:<br><br>*straight pipe, blind-tee, elbow pipe, laminar flow, OpenFOAM CFD, numerical solution, analytical solution* | Pages: 77<br>+ enclosure: **1 CD**<br><br><br>**Stavanger, June 15th 2016** |
|---|---|

# Abstract

The process piping in the refinery plant does not always have straight pipe geometry. The configuration of these pipelines are usually zigzag or snake-like. The pipe fittings or joints including elbow pipes, blind-tee pipes, T-pipes, Y-pipes are found to be common in a refinery. One of the reasons why the pipelines are layed in zigzag or snake-like configuration is because of the limited space for the piping equipment even in the largest refineries.

The aim of the thesis is to study the physical flow inside a pipe with focus on blind-tee and elbow pipes. Laminar flow regime with Reynolds number equals to 1000 is investigated in this study. The analysis utilizes CFD numerical simulations by using OpenFOAM to investigate the physical flow inside the studied pipes. The geometry of the pipes which are used in this study have a diameter (D) of 1 m, and the blind-tee length varied from 1D to 5D. In order to achieve the main objective, there are sub-objectives which need to be carried out. First, the laminar flow analysis of the straight pipe with a length 10D is investigated as the base case of the study. Since the straight pipe is installed before and after the pipe joints in order to attain the fully developed desirable flow profile. Second, the geometry and mesh setup of the studied pipes are created by using Autodesk Inventor, GMSH and SALOME Software, starting with the straight pipe, and then followed by the blind-tee and elbow pipe. Third, the numerical analysis is carried out by performing OpenFOAM CFD simulations. Fourth, the sensitivity studies of different mesh elements, time-steps, and Reynolds number are carried out. Last, the results of the velocity profiles obtained from the numerical simulations are validated with the velocity profiles of laminar flow derived from the analytical solution of classical formula.

Three-dimensional numerical simulations of fluid flow in the straight pipe, blind-tee, and elbow pipe are presented. In addition, the streamline, velocity contour, and pressure contour of the blind-tee and elbow pipe cases are shown. For the straight pipe case, the velocity profile in the pipe agrees well with the analytical solution of classical formula. For the blind-tee and elbow pipe cases, the velocity profile at the 5D from the inlet and 5D from the outlet have been checked for grid convergence studies. It is found that there are flow circulations, which occurs inside the blind-tee. Moreover, for the blind-tee with the tee lengths that are equal to 4D and 5D, fluid deposits would very likely occur, since the velocity inside this tee is very low.

**Keywords**: *straight pipe, blind-tee, elbow pipe, laminar flow, OpenFOAM CFD, numerical solution, analytical solution.*

# Acknowledgement

This master thesis ends my two-year of study in master program of Offshore Technology, specialty Marine and Subsea Technology in University of Stavanger.

I would like to express my deep and sincere gratitude to my supervisor, Prof. Muk Chen Ong, and external supervisor form ROXAR, Emerson Process Management, Dr. Yihan Xing, for introducing this interesting topic to me. Their guidance, patience and encouragement, in addition to the valuable suggestions they gave me throughout the work and final completion of this thesis was over and above the traditional support they provided.

Many thanks to Zhong Li for guiding and introducing me to OpenFOAM and GMSH, also for helping me solve the problem regarding this software.

I would like to thank the University of Stavanger for providing me access to the super computer (Vilje and Gorina). Because without this access, my simulations would not be finished on time.

I want to thank to my fellow Master group friends, Ahmad, Jerry, and Mika. Our discussion and sharing jokes together made the thesis process less frustrating.

The most important thing through this whole process was the supports and prayers I received from my wonderful parents, my sister Diana, and Fahmi Irfan. Thank you for being beside me and giving me moral supports during my study at the University of Stavanger.

For my roommate, Ninis and all my Indonesian friends (Kevin, Chrsiti, Anggi, Reffi, Noto, Pahmi, Rieska, Mas Fikri, Padang, Mas Hendra, Bang Toga, Batch 2013, and Batch 2015): thank you for the wonderful time we spent together. Thank you for being my second family in Stavanger. With you, I did not feel homesick at all. I hope this is not the end of our friendship and wish the best of luck for your future plans. I will definitely treasure our moments we spent together.

And last but not least, I present this thesis to my beloved Mama, and Papa…

Stavanger, June 2016

Utari Cendhy Liestyarini

# Table of Contents

# List of Figures

# List of Tables

# Nomenclature

Symbols

| | |
|---|---|
| $\varepsilon$ | Strain rate tensor |
| $\mu$ | Dynamic viscosity (kg/m.s) |
| $\upsilon$ | Kinematic viscosity (m$^2$/s) |
| $\rho$ | Fluid density (kg/m$^3$) |
| $\tau$ | Shear stress of internal pipe (N/m$^2$) |

Alphabet

| | |
|---|---|
| C | Courant number |
| D | Diameter of the pipe (m) |
| De | Dean number |
| Lh | Entrance length (m) |
| P | Pressure (Pa) |
| $R$ | Radius of the pipe (m) |
| Re | Reynolds number |
| u(r) | velocity profile |
| $V_{avg}$ | Average flow velocity (m/s) |

Abbreviation

| | |
|---|---|
| CFD | Computational Fluid Dynamics |
| OpenFOAM | Open Source Field Operation and Manipulation |
| PISO | Pressure Implicit with Splitting of Operators |
| SIMPLE | Semi-Implicit Method for Pressure Linked Equations |

# Chapter 1.   Introduction

## 1.1.    Background studies

One of the important downstream processes in the petroleum industry is known as oil refinery. According to Gary & Handwerk (1984), oil refinery or petroleum refinery is an industrial process plant where the process of the crude oil into beneficial and commercial products (e.g. petroleum naphtha, diesel fule, gasoline, heting oil, kerosene, asphalt base, and liquified petroleum) are carried out. This industrial process plant has a complex configuration with large number of tanks and vessels, various pipes sizes, fire heaters, pumps and compressors, instrumentation and control systems, and many more (Olsen, 2014). Figure 1.1 exhibits one example of an oil refinery plant which is located in Algeria and owned by Sonatrach. It has capacity of CDU (Crude Distillation Unit) ½ Total : 18 Million metric tonnes per annum (MTPA). The construction of this oil refinary plant was completed in 2015.



**Figure 1.1.** Example of Oil Refinery Plant by Samsung Engineering (Samsung-Engineering, 2013)

The types of pipeline in the oil refinery plant consist of not only crude oil lines but also gas lines, condensation lines, and steam lines. These pipelines are built with different material properties and sizes depending on what they carry. The process piping in the refinary plant does not always have straight pipe geometry. The configuration of these pipelines are usually zigzag or snake-like. The pipe fittings or joints such as elbow pipe, blind-tee pipe, T-pipe, Y-pipe, and many more are common to be found in this plant (see Figure 1.2). One of the reasons why the pipelines are layed in zigzag or snake-like configuration is

because of the limited space for the piping equipment even in the larger refineries. The example of piping fittings in the refinery plant is shown in Figure 1.2.
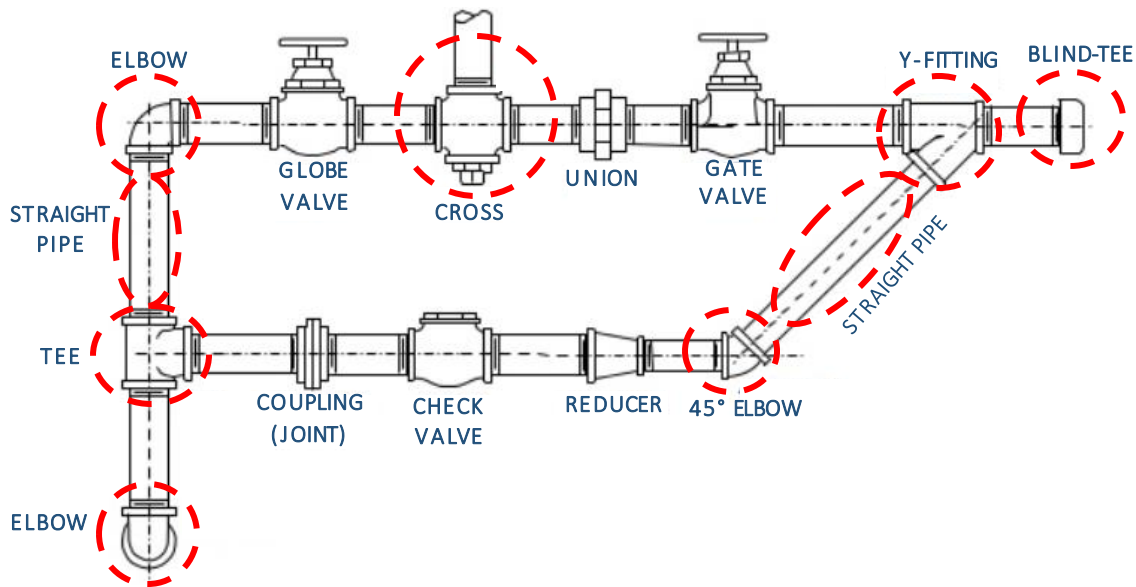


**Figure 1.2.** Schematic Diagram of Pipe Fittings (Shearer, 2014, p. 159)

At the connections or the joint parts of the pipelines, the fluid flow will behave differently from the flow of the fluid in the straight pipe. The physical flow inside these joints needs to be studied since there are some concerns regarding engineering design. First, it should be investigated whether there will be any deposits inside the pipe joints, since it may lead to erosion and corrosion of the pipe. Second, it should be checked whether the flow (especially multiphase flow) is well mixed during and after crossing the pipe fittings. Third, the impact of blind-tee configuration changes to the characteristics of the pipe flow needs to be observed.



**Figure 1.3.** Blind-tee Pipe (Left) (Prinsco, 2016) and Elbow Pipe (Right) (Pipestock, 2004)

In order to have good understanding about the physical flow inside pipe fittings or joints, this thesis will focus on the study of the behavior of internal flow in the blind-tee and elbow pipes. The internal flow is

simulated by OpenFOAM CFD modelling with laminar flow analysis. The result of this study is expected to enable the oil and gas industry to obtain a better understanding of the physics and characteristics of the flow pattern inside the blind-tee pipe and elbow pipes.

## 1.2. Scope of work

This thesis is written in collaboration with ROXAR, Emerson Process Management to study the internal pipe flow in the blind-tee and elbow pipes which are found in the process piping. The thesis utilizes OpenFOAM CFD modeling to investigate the physical flow numerically inside the studied pipe. Moreover, Newtonian, incompressible fluid and laminar flow are setup for the initial flow inside the studied pipes. The main objective of this thesis is to model the pipe flow numerically, and analyze the physics and characteristics of the flow pattern inside the blind-tee and elbow pipes. In order to achieve this objective, the following sub-objectives need to carry out:

- Conduct the laminar flow analysis of the straight pipe as the baseline of this study. Since the straight pipe is installed before and after the pipe joints in order to attain the fully developed desirable flow profile.
- Create the geometry and mesh of the studied pipes by using Autodesk Inventor, GMSH, and SALOME Software, starting with the straight pipe and then the blind-tee and elbow pipes.
- Carry out the numerical analysis by utilizing OpenFOAM CFD modelling
- Carry out the sensitivity studies of different mesh elements, time-steps, and Reynolds numbers.
- Validate the results of the velocity profile obtained from the numerical solution with the analytical solution of classical formula for laminar flow velocity profile.

Figure 1.4 exhibits the flow chart of the general scope of work of this thesis:
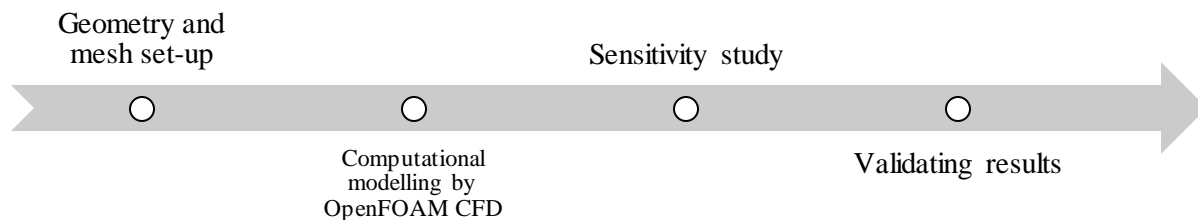


**Figure 1.4.** Flow Chart of the Scope of Work

3

## 1.3.    Related published works

This section discusses about the previous works which have been published. These published works were taken from some journal papers which discuss the laminar flow regime inside the pipe, as well as the numerical and analytical studies of the flow inside the straight and curved pipes. For the characteristic of flow inside the pipe fittings, such as T-pipe, were discussed in the previous work. However, to the author's knowledge, the physics of the flow inside the blind-tee have not yet been discussed in any publications.

<u>Laminar Flow Regime</u>

Hornbeck (1964) investigated the laminar flow of an incompressible fluid in the pipe inlet with a numerical solution. This numerical solution was utlizing finite difference marching procedure in which the velocities and pressure at any position in the pipe was calculated by using values obtained upstream from the particular point. It was recognized that the numerical technique approach could provide a closer approximation to the basic equation of a fluid motion. He concluded that the result exhibited significant difference for both velocity profiles and development lengths between this numerical solution and the previous study. It was because in the previous work by Campbell and Slattery (Campbell & Slattery, n.d. cited in Hornbeck, 1964, p.224 ), the flat central core was assumed to be installed in the central of the pipe (Radius (R) =0) until R = 0.9 in the almost entire entrance region, while in his study no such assumption was used. Because of this flat core, the velocity at the centerline (R = 0) increased slowly than the velocity derived from numerical solution. However, the increased velocity at R = 0.6 was more rapid in the previous work. The velocity results from both solutions at R = 0.9 were same. This was because the flat core did not effect the velocity in this region.

Friedmann et al., (1968) studied the laminar flow of a homogeneous viscous liquid inside a pipe with different low and moderate Reynolds number (Re) in the range of 0 to 500. They calculated the velocity distribution and velocity profiles of flow numerically using the finite difference equations. The notation of the velocity which represented axial velocity component was defined as u and v. Moreover, x was defined as axial coordinate and r as radial coordinates. The results of this calculation were compared with other published literature. For the Reynolds number Re = 200 and 500, the velocity distribution curve of their study agreed well with the previous work which was done by Nikuradse's experiment (Prandtl & Thetjens, 1957, p. 27, cited in Friedmann et al, 1968, p.431) for the downstream region (2x/Re ≤ 0.07). However, the fit was worse for larger values of x. There was "kink effect" which occured in the velocity profile at small x which the location of x = 0 is at the inlet of the pipe. This effect was also detected by Brandtl and Gillis

(Brandtl and Gillis, 1964 cited in Friedmann et al., 1968, p.432) and by Wang and Longwell (Wang and Lognwell, 1964 cited in Friedmann et al., 1968, p.432) on the previous studies of flow in a straight channel.

Flow inside straight pipe

Cade et al. (2010) analyzed the different flow parameters of natural gas, its velocity and pressure distribution inside the straight pipes which had elliptical and circular cross sections. The fluid flow which was studied was a three-dimensional mathematical model. The results were obtained by using CFX-3D CFD. The characteristic parameters setup of the elliptical and circular cross section pipes were defined as ratio of $L_1$ and $L_2$. Where $L_1$ was the radius of the cross-section in the horizontal axis, and $L_2$ was the radius of the cross-section in the vertical axis. A circular pipe with dimensions $L_1 = L_2 = 0.173205$ m and an elliptical pipe with dimensions $L_1 = 0.1$ m and $L_2 = 0.3$ m were studied. The inlet velocity which was used for all pipes was 0.1 m/s. In their study, the pressure drop which was occurred in circular pipe was about 0.014347 Pa wheras in elliptical pipe was about 0.021516 Pa. Thus, with the equivalent mass flow rate, the pressure drop inside the elliptical pipe is 50% higher than in the circular pipe. While, the other analysis was conducted on the other two pipes which the first pipe was a circular pipe with dimensions $L_1 = L_2 = 0.1$ m (pressure drop = 0.032060 Pa) and the second pipe was elliptical pipe with dimensions $L_1 = 0.1$ m and $L_2 = 0.15$ m (pressure drop = 0.025226 Pa). With an inlet velocity of 0.1 m/s, it was found that the volumetric flow rate in the elliptical pipe is 50% higher than in a circular pipe. Hence, it could be concluded that the velocity of natural gas in pipes was influenced by the cross section area of the pipe. The higher the aspect ratio ($L_2/L_1$), was the longer the hydrodynamic entrance length to achieve a fully developed flow.

Flow inside T-junction and curved pipe

Vasava (2007) studied the flow properties inside the T-junction pipe, and its head loss. Moreover, he compared the head loss which was obtained from the numerical simulation with the head loss calculated from the analytical solution of classical formula which was obtained by previous studies such as A. Vazsonyi (Tennekes & J.L., 1992), A. Gardel (Foias, et al., 2001), and V. Curic (Temam, 1984). The FLUENT CFD software and Comsol Multiphysics was used as the numerical simulation tools. Water with normal properties at room temperature was considered as the fluid for this study. He concluded that in the case of combining flow, the head loss difference between his study obtained by Comsol Multiphysics and the classical formula obtained from Vazsonyi (Tennekes & J.L., 1992, cited in Vasava, 2007, p.50), A. Gardel (Foias et al., 2001, cited in Vasava, 2007, p.50), and V. Curic (Temam, 1984, cited in Vasava, 2007, p.50) were in the range of 3.2 to 5.1%. In addition, in the case of dividing flow, the difference was in the range of 4.5 to 5.5%. In the case where angle of T-juntion was varied from 87 degrees to 93 degrees, the

5

difference was in the range of 4.6% to 6.7%. These errors occurred due to the limitation of software to handle complicated flow conditions (e.g. turbulence flow) and to model rough inner surface of pipes. The next analysis was comparing the head loss result obtained by FLUENT CFD software with the classical formula derived from Gardel's formula (Foias et al., 2001, cited in Vasava, 2007, p.50) and Vazsonyi's formula (Tennekes & J.L., 1992, cited in Vasava, 2007, p.50). It was observed that for the combining flow case, the difference was in range of 3.2% to 5%, and for dividing flow cases, the differences was in range of 4.5% to 6%. This classical formula derived from Vazsonyi (Tennekes & J.L., 1992), A. Gardel (Foias, et al., 2001) was less precise since the pipe roughness was not considered. It was conluded form this study that FLUENT CFD software was a better alternative for heavy and precise simulations since FLUENT was able to model turbulence flow with various κ-Epsilon models.

Shirayama & Kuwahara (1987) analyzed finite difference procedure of numerical solution in order to solve the Navier-Stokes equations of the laminar and incompressible flow inside a curved pipe. The method of consecutive over-relaxation was used to solve pressure equation. The time integration for this study was utlizing the Euler implicit scheme. The spatial derivatives terms were solved by the central differences approximation. While the nonlinear terms were approximated by a third-order upwind scheme. The Japanese supercomputers, such as Fujitsu VP 200, VP 400, and NEC SX/2 were used to execute the simulation. The governing equations of Navier-Stokes were generated by using enough number of grid points. The computaion domains were circular pipe with straight pipe in the inlet and outlet. Thus, This equations were solved in the cylindrical coordinate system (r, θ, z). The studied circular pipes had radius of 0.05, 0.143, and 0.148 with the Dean number varied from 183 to 3847. Dean number is the non-dimensional number for the ratio of viscous force acting on a fluid which flows in a curved pipe to the centrifugal force (see sub-chapter 2.6). They observed that two symmetric recirculating regions occurred in low-Dean-number flows. As the Dean number rised, this secondary motions encouraged the seperations of cross-sectional flow. Furthermore, in high-Dean number flow, the main flow seperated thus caused unsteady flow field. These recirculation flows occur when it was subjected to the viscous fluid element response to the unstable between the acceleration of centripetal and pressure gradient of the cross section encouraged by lateral curvature of main flow. Even so, there were some occurances of recirculation due to the main flow seperation.

## 1.4.    Outline of thesis

➢ Chapter 2. Theory.

This chapter provides the theoretical reviews about the flow inside the pipe, the laminar flow regime, and the developed velocity profile in laminar flow regime.

➢ Chapter 3. Computational Fluid Dynamics (CFD)

This chapter describes about the Computation Fluid Dynamics, the introduction of OpenFOAM, and the governing equations which are used in this thesis.

➢ Chapter 4. Numerical Set up

This chapter describes the geometry model, mesh set-up, boundary conditions, and solver set-up that are utilized for this thesis.

➢ Chapter 5. Straight Pipe Case

This chapter discusses and exhibits the results of numerical solution of the laminar flow inside a typical straight pipe.

➢ Chapter 6. Blind-tee and Elbow Pipe Case

This chapter discusses and exhibits the results of numerical solution of the laminar flow inside typical blind-tee and elbow pipes.

➢ Chapter 7. Conclusion and Recommendation for Further Work

This chapter describes the conclusion of this study and gives recommendation of what should be done and what can be done for future works regarding the present study.

# Chapter 2.   Theory

## 2.1.     Characteristics of flow

According to Cengel & Cimbala (2014), the categorization of fluid flow is defined as external and internal flow. This classification is based on whether the fluid is flowing over a surface or inside the channel or pipe. For this thesis, the characteristics of flow inside the pipe will be studied. Therefore, all of the discussed theories below are about the characteristics of internal fluid flow.

## 2.2.     The concept of laminar and turbulent flows

According to Cengel & Cimbala (2014), the best way to distinguish the flow regime is by observing the injected dye into the middle of the flow stream. When the dye is injected into the steady flow stream with low velocity, it exhibits straight and smooth line. On the other side, it shows sudden change on the pattern as the velocity increases. As result, the dye will become zigzag swiftly and unsystematically in very high velocities. From this illustration, it can be recognized that the dye which displays steady and smooth lines, are categorized as laminar flow. Furthermore, the dye that shows randomly patterns, are categorized as turbulent flow.

This experiment of the injected dye to the flow stream of fluid has been conducted by the British engineer, Osborne Reynolds (1842-1912) over a century ago. He discovered that the laminar flow regime is specified as smooth streamlines with highly ordered motion and the turbulent flow regime is identified by velocity fluctuations with highly disordered motion. The picture of the dye injection experiment can be found in Figure 2.1.
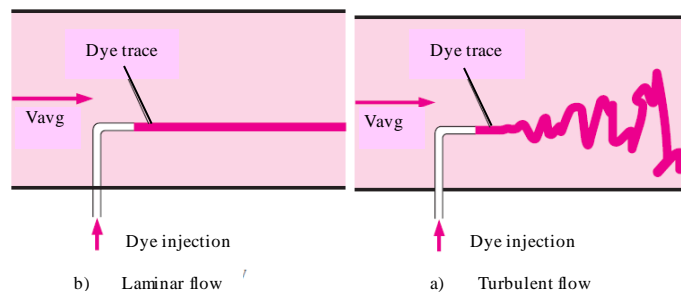


**Figure 2.1.** "The Behavior of Colored Fluid Injected Into the Flow in Laminar and Turbulent Flows in a Pipe" (Cengel & Cimbala, 2014, p. 349)

Figure 2.1 shows the different behaviors of laminar and turbulent flow. The turbulent flow exhibits a great mixture of the fluid. This event is the consequence of the prompt fluctuations which increases the transfer of the momentum between fluid particles. This momentum transfer phenomena can increase the friction force on the pipe wall and extends its maximum at full turbulent. This is because at fully turbulent, the momentum between fluid particles becomes very high which leads to the large friction force on the pipe wall (Cengel & Cimbala, 2014).

## 2.3.    Reynolds number

In principle, the flow regime is based on the ratio of inertial forces to viscous forces in the fluid. This ratio is known as Reynolds Number (Cengel & Cimbala, 2014). Thus, the equation of Reynolds number for the flow inside the circular pipe is:

$$Re = \frac{Inertial\ forces}{Viscous\ forces} = \frac{V_{avg}\ D}{v} = \frac{\rho V_{avg}\ D}{\mu} \qquad (2\text{-}1)$$

Where $V_{avg}$ = average flow velocity (m/s), D = the characteristic length of the geometry or diameter of the pipe (m), $v = \frac{\mu}{\rho}$ = kinematic viscosity of the fluid (m²/s).

Mostly, in the empirical condition, the flow regime inside the circular pipe can be defined as laminar flow with $Re \lesssim 2300$; transitional flow with $2300 \lesssim Re \lesssim 4000$; and turbulent flow with $Re \gtrsim 4000$ (Cengel & Cimbala, 2014).

## 2.4.    Entrance region

At the inlet, the fluid which flows uniformly across the cross-section of a pipe, will not be effected by the friction between the pipe's wall and the fluid. However, as the flow moves along in the pipe, this friction wall effect moves toward the center of the pipe until the velocity profile becomes stable (Bengston, 2010). Figure 2.2 shows the illustration of the entrance region.
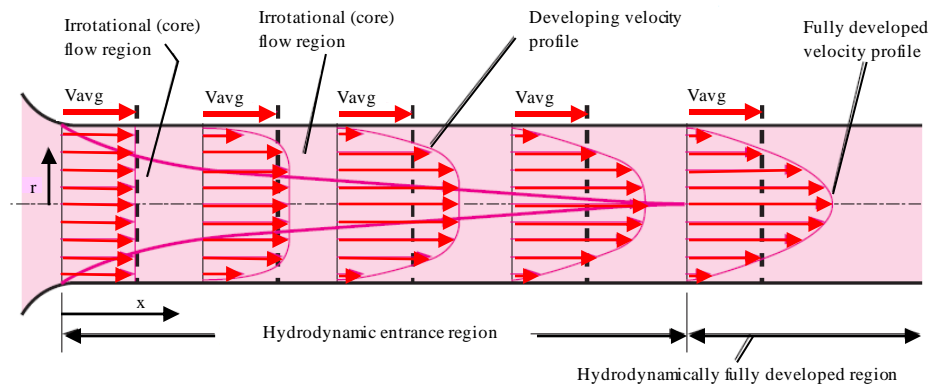
**Figure 2.2.** Entrance Region Diagram (Cengel & Cimbala, 2014, p. 351)

Figure 2.2 shows some terms which are typically used for flows of fluid inside the pipe. The velocity boundary layer (boundary layer) is the flow zone where the fluid viscosity generates the viscous shearing forces effects. The flow in the pipe is separated into two zones, which are the boundary layer region and the irrotational (core) flow region. In the boundary layer region, the alteration of viscous effects and the velocity are significant. However, in the irrotational (core) flow region the frictional effects is ignored and in the radial direction, the velocity stays constant.

As the flow proceeds through the pipe, the thickness of the boundary layer expands in the flow direction until it achieves the center of the pipe, therefore the fluid will fill the entire pipe. The hydrodynamic entrance region is the zone from the pipe inlet to the point which the boundary layer meets in the pipe center. The length of this region is hydrodynamic entrance length (Lh). The zones where the velocity profile develops is called hydro-dynamically developing flow and the region beyond the developing flow is the hydro-dynamically fully developed region. In this region, the velocity profile has already fully developed and stays constant or unchanged. The flow can be recognized as fully developed when its temperature profile keeps unchanging. The developed velocity profile between laminar flow and turbulent flow are different. The developed velocity profile in laminar flow can be identified by the parabolic profile. While, in the turbulent flow the profile is slightly flatter because of the eddy motion and great mixing in the radial direction (Cengel & Cimbala, 2014). The illustration of developed flow of laminar and turbulent flow, can be seen in the Figure 2.3.
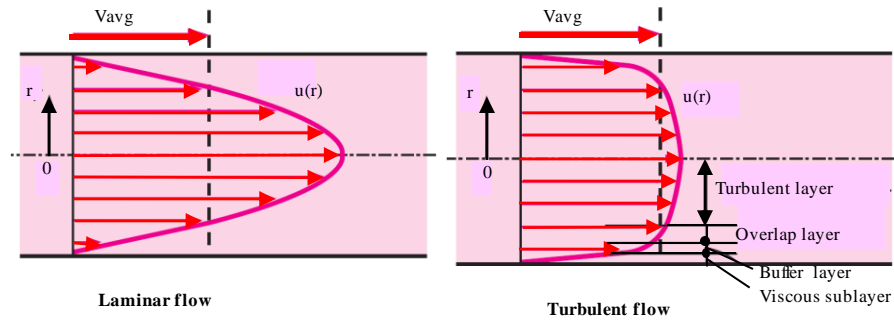
**Figure 2.3.** Velocity Profile of Developed Flow (Cengel & Cimbala, 2014, p. 365)

According to Cengel & Cimbala (2014), the hydrodynamic entrance length (Lh) or entry length for laminar flow is expressed as

$$L_{h,laminar} \cong 0.05 \, Re \, D \qquad (2\text{-}2)$$

It means that the distance from the inlet of the pipe until the point where the wall shear stress (or the friction factor) achieves about 2% of the fully developed value is approximately 5% of the Reynolds number times the diameter of the pipe (see Figure 2.4).
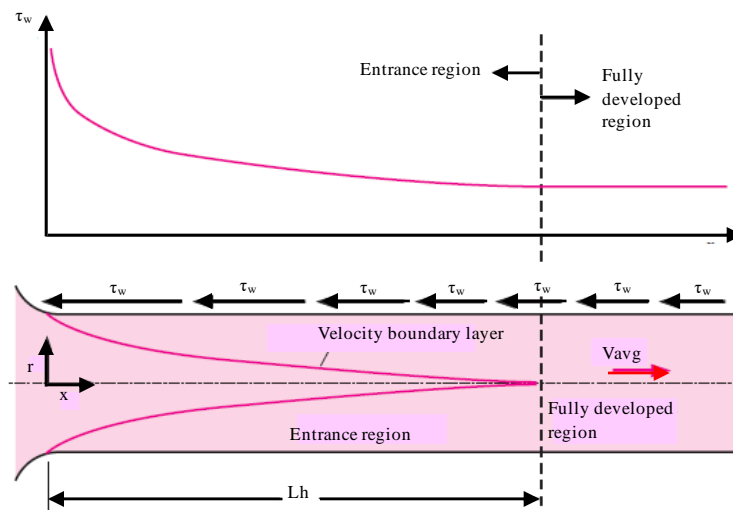


**Figure 2.4.** "The Variation of Wall Shear Stress in The Flow Direction for Flow in a Pipe from the Entrance Region into the Fully Developed Region" (Cengel & Cimbala, 2014, p. 352)

11

In the turbulent flow, the entrance length is shorter than in the laminar flow. Moreover, the dependency on the Reynolds number is very small and usually it is negligible in the engineering practice. In the practice, the effect of the entrance flow is less important beyond a pipe length that equals 10 times its diameter (L=10D). Thus, the approximation of the hydrodynamic entry length in turbulent flow is expressed as:

$$L_{h,turbulent} \cong 10\ D \tag{2-3}$$

## 2.5.  Laminar flow

Since this thesis is only focusing on the laminar flow region, thus the further background theories which are discussed in this chapter are about laminar flow region. The scope of laminar flow in this section is the laminar flow which is steady, incompressible, and flowing inside a pipe. Considering the characteristic of laminar flow, the fluid particle in this flow regime will move at steady axial velocity throughout the streamline. Thus in the flow direction, the velocity profile will stay the same. In this flow regime, the velocity component which locates in the normal direction to the pipe axis is zero. Acceleration does not occur since it is steady and fully develop flow (Cengel & Cimbala, 2014).

The velocity profile of laminar flow is derived from the relationship between the pressure force at the centroid of the surface and the surface area, and the viscous forces which act on the pipe wall. The following explanations are the steps how to obtain velocity profile in laminar flow regime according to Cengel & Cimbala (2014):

- The force balance on the volume element in the flow direction:

$$(2\pi\ r\ dr\ P)_x - (2\pi\ r\ dr\ P)_{x+dx} + (2\pi\ r\ dx\ \tau)_r - (2\pi\ r\ dx\ \tau)_{r+dr} = 0 \tag{2-4}$$

The terms of the Equation (2-4) can be seen in Figure 2.5.
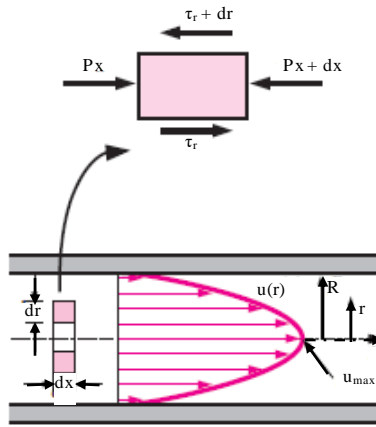
**Figure 2.5.** Free-body Diagram of a Ring-shaped Differential Fluid Element where r is Radius, dr is Thickness, and dx is Length (Cengel & Cimbala, 2014, p. 353).

- In the horizontal pipe, the viscous and pressure forces of fully develop flow are balance each other. By dividing Equation (2-4) with $2\pi dr dx$:

$$r\frac{P_{x+dx} - P_x}{dx} + \frac{(r\tau)_{r+dr} - (r\tau)_r}{dr} = 0 \tag{2-5}$$

Taking the limit as dr, dx → 0, becomes:

$$r\frac{dP}{dx} + \frac{d(r\tau)}{dr} = 0 \tag{2-6}$$

Then, replace $\tau = -\mu\left(\frac{du}{dr}\right)$ and take μ as a constant:

$$\frac{\mu}{r}\frac{d}{dr}\left(r\frac{du}{dr}\right) = \frac{dP}{dx} \tag{2-7}$$

- For flow in pipe, the value of du/dr is negative. This negative sign should be used in order to obtain the positive value of τ. In other words, du/dr = -du/dy since y = R-r. In Equation (2-7), dP/dx is defined as constant. This can be confirmed by solving the force balance (Equation (2-8)) on a volume element with radius R and thickness of a slice of pipe (dx):

$$\pi R^2 P - \pi R^2(P + dP) - 2\pi R dx\, \tau_w = 0 \tag{2-8}$$

Which gives:

$$\frac{dP}{dx} = -\frac{2\tau_w}{R} \tag{2-9}$$

The Equation (2-9) shows that the $\tau_w$, is constant because of the unchanging viscosity and velocity profile in the fully developed region. Here $\tau_w$ is defined as pipe shear stress (N/m²). The Equation (2-7) is integrated twice, becomes:

$$u(r) = \frac{1}{4\mu}\left(\frac{dP}{dx}\right) + C_1 \ln r + C_2 \tag{2-10}$$

From equation above, the velocity profile can be obtained by applying the boundary conditions:

1) $\frac{\partial u}{\partial r} = 0$ at $r = 0$ → since it is symmetry about the centerline
2) u = 0 at r = R → no slip condition at the wall surface

Thus, it gives:

$$u(r) = -\frac{R^2}{4\mu}\left(\frac{dP}{dx}\right)\left(1 - \frac{r^2}{R^2}\right) \tag{2-11}$$

It can be concluded form Equation (2-11) that the velocity profile for laminar flow is parabolic with the maximum velocity is located at the centerline and the minimum velocity (zero) at the wall of the pipe. Moreover, for any r, the axial velocity shall be positive hence the pressure gradient (dP/dx) must be negative.

- The average velocity for incompressible flow in circular pipe with radius R is expressed as:

$$V_{avg} = \frac{\int_{A_c} \rho u(r) dA_c}{\rho A_c} = \frac{\int_0^R \rho u(r) 2\pi r \, dr}{\rho \pi R^2} = \frac{2}{R^2}\int_0^R u(r) r \, dr$$
$$= -\frac{2}{R^2}\int_0^R \frac{R^2}{4\mu}\left(\frac{dP}{dx}\right)\left(1 - \frac{r^2}{R^2}\right) r dr = -\frac{R^2}{8\mu}\left(\frac{dP}{dx}\right) \tag{2-12}$$

- Then, combining the last two equation generates the velocity profile:

$$u(r) = 2 V_{avg}\left(1 - \frac{r^2}{R^2}\right) \tag{2-13}$$

When substituting r = 0, it gives $u(r) = 2 V_{avg}$. Hence, it can be said that the average velocity in fully developed laminar pipe flow is one half of the maximum velocity.

## 2.6.  Dean number

The effects of fully developed flow in a curved pipe have been reviewed in the several previous studies. In the Dean's investigation of flow inside a curved pipe, he discovered solutions to depict the behavior of the fluid in the central core which flowed more promptly than the average flow. Moreover, this flow was pushed away from the center of the curvature by the centrifugal action. The fluid which flows slowly in the wall region, would move towards the center of the curvature where pressure is lower (Spedding, et al., 2004). Thus, in order to give a non-dimensional number from mathematical expression for the ratio of the viscous force acting on a fluid which is flowing in a curved pipe to the centrifugal force, Dean number (De) is given (Shirayama & Kuwahara, 1987):

$$De = Re\left(\frac{R}{A}\right)^{0.5} \tag{2-14}$$

Where Re is the Reynolds number, R is the radius of the cross section, and A is the outside radius of the curve. The ratio of R/A is shown in Figure 2.6.



.
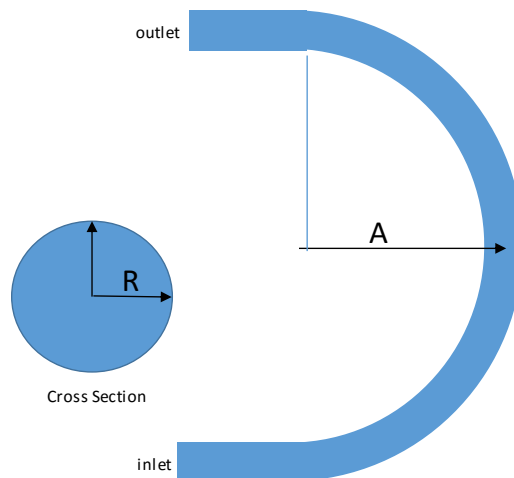
**Figure 2.6.** Illustration of R/A Ratio (Shirayama & Kuwahara, 1987, p. 52)

# Chapter 3.  Computational Modelling

## 3.1.  Computational Fluid Dynamics (CFD)

Computational Fluid Dynamic is a computational tool which is beneficial in constructing and solving the equations which are used to model the flow movement (Patel, 2013). This is based on the consideration that these equations are complex to solve analytically. Principally, CFD is utilized to obtain close estimation of the flow motions and characteristics with the reality. The difference between this computational modelling and experimental studies in studying the flow model is that by using CFD, one can have better understanding about the flow physics than in the laboratory. Since in the laboratory many uncertainties in the experimental tools might occur. The other advantages of using CFD are (Tu et al., 2007):

1. CFD has possibilities in resolving various complicated experiments problem which cannot be solved with available tools in the laboratory.
2. CFD is efficient to be used since it reduces the operational time and the costs of designs and productions, unlike the experimental based approach.
3. CFD is capable of covering the limitation of analytical approach in solving the various complex flow problems.
4. CFD offers more detailed, visualized, and comprehensive information and results than analytical and experimental in fluid dynamics.

Like any other numerical computational programs, one cannot directly trust the result which is presented in the CFD. Sometimes, numerical errors might occur in the computations which lead to the significant outcome between computed result and the reality. According to Tu et al. (2007), the huge amount of data of unsteady flows which is computed by using CFD, will be expressed in the very nice visualization, such as vectors, contours, and animated movies. The result which might look exceptional, may not represent the real flow behavior if the computation is not completely correct. Consequently, the user should have an understanding in analyzing and making critical assessment on the generated results.

CFD consists of three main elements, which are Pre-processor, Solver, and Post-processor. These elements should be fulfilled in order to obtain the accurate solution. Figure 3.1 is the flow-chart diagram that shows the connections between those three main elements according to Tu et al. (2008):
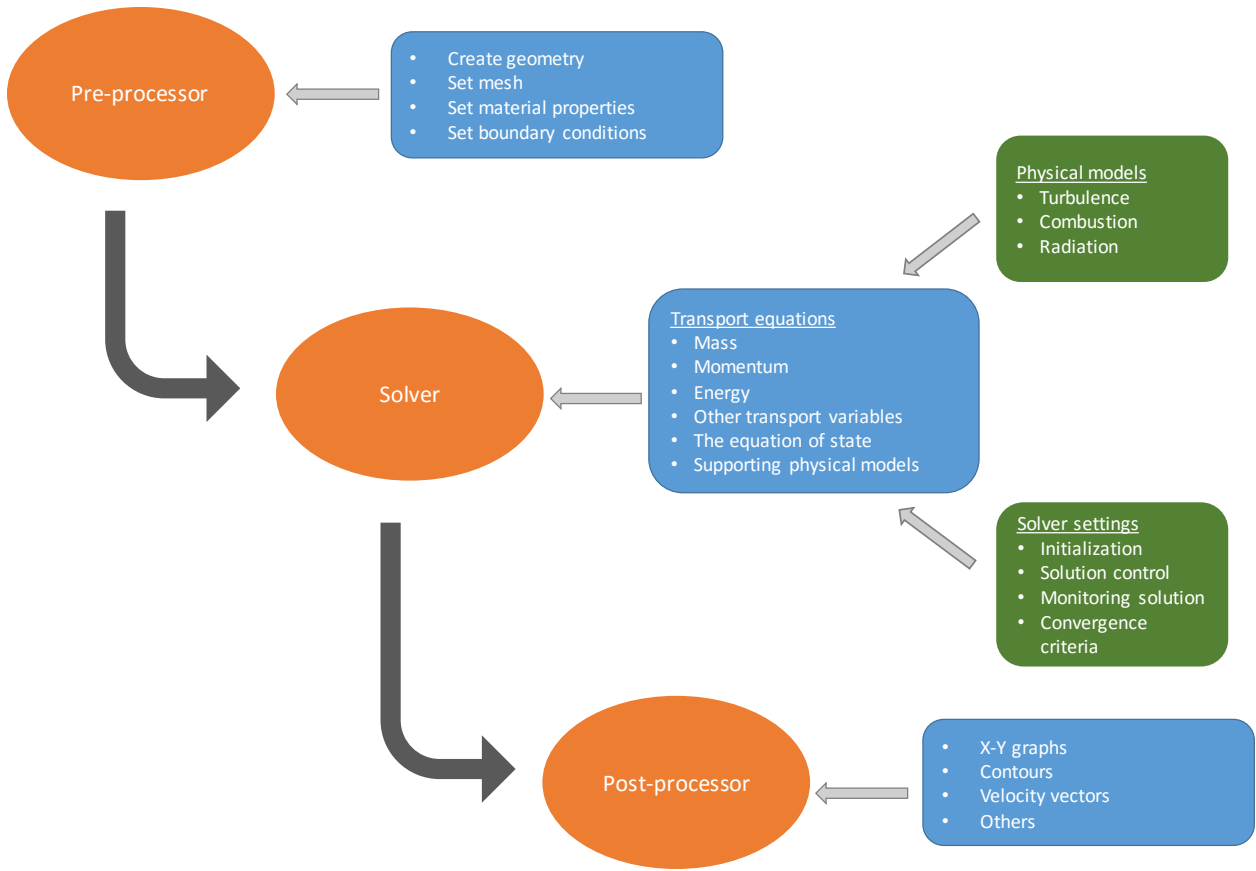
**Figure 3.1.** Flow Chart of CFD Main Elements (Tu et al., 2008, p.33)

The flowchart of CFD main elements which are explained in details in point (i) through (iii) is according to Mehul (2013).

(i)      Pre-processing

Pre-processing is the initial step in the CFD simulation process which is the stage where the geometry is created. The geometry needs to be designed in a way that represents the observed geometry in reality. The fluid domain of interest shall be defined properly. Then, this domain of interest will be divided into smaller segments, e.i. mesh generation set up. Hence, several tasks which must be done in pre-processing stage are creating the geometry domain, setting up the mesh and material properties, also setting up the boundary conditions. In addition, the well-known pre-processing software are Gridgen, CFD-GEOM, ANSYS Meshing, ANSYS ICEM CFD, SALOME, GMSH, and TGrid.

(ii)      Solver

In this stage, the fluid material properties, flow physics model, and boundary conditions are set in order to be solved using the computational program. This stage can be done after the problem physics are identified

correctly. Some examples of physics model are turbulence, combustion, and radiation. These physics model will be solved by the transport equations of mass, momentum, energy, other transport variables, the equation of states, and supporting physical models.

This stage consists of a number of settings, such as initialization, solution control, monitoring solution, and convergence criteria. Several commercial software solutions which are well known: ANSYS FLUENT, ANSYSCFX, Star CCM, CFD++, and OpenFOAM. The governing equations problems which are associated to flow physics, can be solved using these software solutions.

(iii)    Post-processing

This stage is utilized to investigate the results which are obtained from the previous stage. Different methods can be used to achieve appropriate and convenient graphical presentation and report. These methods include plots of contour, plots of vector streamlines, and data curve. The common post-processing software solutions which are available in the market are ANSYS CFD-Post, En-Sight, FieldView, ParaView, and Tecplot 360.

## 3.2.    The Governing equations

Principally, the numerical solution by CFD solves the governed equations of mathematical models. These mathematical models are the governing equations of fluid flow which are based on the conservation laws of physics. There are four governing equations in order to solve the velocities (in three directions) and the pressure in the fluid flow problem. The following sub-chapters are the discussion of these governed equations.

### 3.2.1.  Conservation of mass

According to Versteeg & Malalasekera (1995, p.11), the conservation of mass for fluid element is based on the mass balance:

*"Rate of increase of mass in fluid element = Net rate of flow of mass into fluid element"*

The rate of increase of mass in the fluid element is expressed as:

$$\frac{\partial}{\partial t}(\rho \delta x \delta yz) = \frac{\partial \rho}{\partial t}\rho \delta x \delta yz \qquad (3\text{-}1)$$

Next step is calculating the mass flow rate which is crossing a face element. The mass flow rate is the product of density, area and the velocity component normal to the face (see Figure 3.2).

18
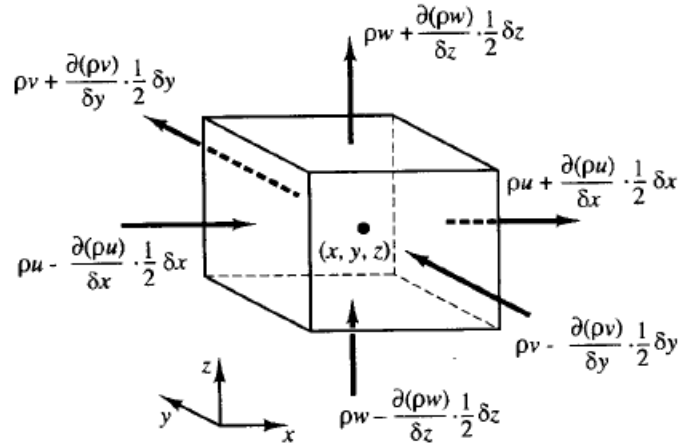
**Figure 3.2.** "The Mass Flows in and out Fluid Element" (Versteeg & Malalasekera,1995 p.12)

According to Figure 3.2, the net rate of flow of mass into element across its boundaries is written as:

$$
\left(\rho u - \frac{\partial(\rho u)}{\partial x}\frac{1}{2}\delta x\right)\delta y \delta z - \left(\rho u + \frac{\partial(\rho u)}{\partial x}\frac{1}{2}\delta x\right)\delta y \delta z + \left(\rho v - \frac{\partial(\rho v)}{\partial y}\frac{1}{2}\delta y\right)\delta x \delta z
$$
$$
- \left(\rho v + \frac{\partial(\rho v)}{\partial y}\frac{1}{2}\delta y\right)\delta x \delta z + \left(\rho w - \frac{\partial(\rho w)}{\partial z}\frac{1}{2}\delta z\right)\delta x \delta y \qquad (3\text{-}2)
$$
$$
- \left(\rho w + \frac{\partial(\rho w)}{\partial z}\frac{1}{2}\delta z\right)\delta x \delta y
$$

The Equation (3-2) shows that flows which are heading into the element, produce an increase of mass in the element. Hence, their signs are positive. While, the flows leaving from the element are signed negative. The Equation (3-2) is arranged to the left hand sign of equals sign and then it is divided by the element volume $\delta x \delta y \delta z$:

$$
\frac{\partial}{\partial t} + \frac{\partial(\rho u)}{\partial x} + \frac{\partial(\rho v)}{\partial y} + \frac{\partial(\rho w)}{\partial z} = 0 \qquad (3\text{-}3)
$$

Or can be written in simpler vector notation:

$$
\frac{\partial \rho}{\partial t} + \nabla \cdot (\rho \cdot \vec{u}) = 0 \qquad (3\text{-}4)
$$

The Equation (3-4) is defined as unsteady, three-dimensional mass conservation or continuity equation at a point in a compressible fluid. If the flow is assumed to be steady state, means that:

$$\frac{\partial}{\partial t} = 0 \tag{3-5}$$

When the fluid is incompressible, the density is set to be constant, then the mass balance is given as:

$$\frac{\partial u}{\partial x} + \frac{\partial v}{\partial y} + \frac{\partial w}{\partial z} = 0 \tag{3-6}$$

According to (Cengel & Cimbala, 2014), in the cylindrical coordinates, the continuity equation is expressed as:

$$\frac{1}{r}\frac{\partial (ru_r)}{\partial r} + \frac{1}{r}\frac{\partial (u_\theta)}{\partial \theta} + \frac{\partial (u_z)}{\partial z} = 0 \tag{3-7}$$

In the vector notation can be written as:

$$\vec{\nabla}.\vec{u} = 0 \tag{3-8}$$

### 3.2.2. Conservation of momentum

According to Versteeg & Malalasekera (1995, p.14), the momentum equation is based on the Newton's second law which is :

*"Rate of increase of momentum of fluid particle = Sum of forces on fluid particle"*

Firstly, the x-components of the forces due to pressure (p) and the component of stresses ($\tau_{xx}, \tau_{xy}, \tau_{xz}$) are considered. As shown in Figure 3.3, the magnitude of a force from a surface stress is the result of the product of the stress and area.
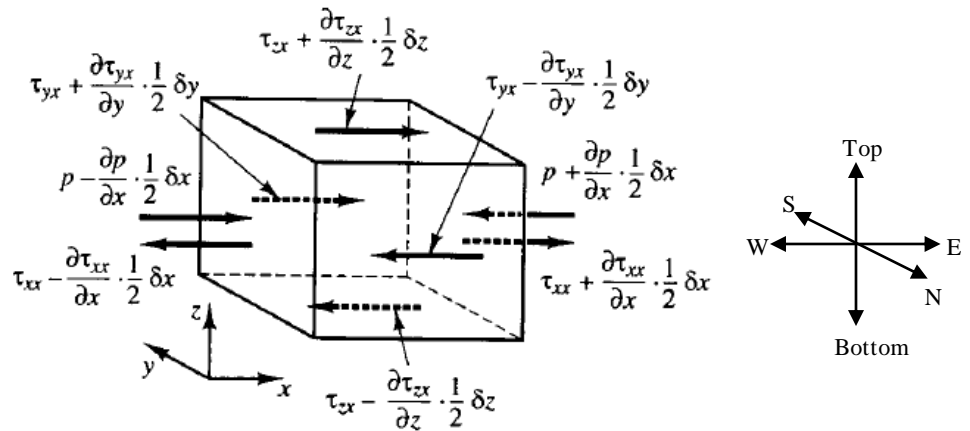


**Figure 3.3.** "Stress Components in X-direction" (Versteeg & Malalasekera, 1995, p.15)

As shown in Figure 3.3, the forces which are aligned with the direction of the x-coordinate, are given in positive sign. On the other hand, the negative sign is given to the Forces which are in the opposite direction from the x-coordinate. Thus, it can be concluded that the sum of the force components which are acting in the x-direction on the fluid element is the net force in that direction (Versteeg & Malalasekera, 1995).

The force components acting on the faces (E, W) are given as:

$$\left[\left(p - \frac{\partial p}{\partial x}\frac{1}{2}\delta x\right) - \left(\tau_{xx} - \frac{\partial \tau_{xx}}{\partial x}\frac{1}{2}\delta x\right)\right]\delta y\delta z$$
$$+ \left[-\left(p + \frac{\partial p}{\partial x}\frac{1}{2}\delta x\right) + \left(\tau_{xx} + \frac{\partial \tau_{xx}}{\partial x}\frac{1}{2}\delta x\right)\right]\delta y\delta z \tag{3-9}$$
$$= \left(-\frac{\partial p}{\partial x} + \frac{\partial \tau_{xx}}{\partial x}\right)\delta x\delta y\delta z$$

The net force components in the x-direction acting on the faces (N, S) are written as:

$$-\left(\tau_{yx} - \frac{\partial \tau_{yx}}{\partial y}\frac{1}{2}\delta y\right)\delta x\delta z + \left(\tau_{yx} + \frac{\partial \tau_{yx}}{\partial y}\frac{1}{2}\delta y\right)\delta x\delta z = \frac{\partial \tau_{yx}}{\partial y}\delta x\delta y\delta z \tag{3-10}$$

The net force components in the x-direction acting on the faces (Top, Bottom) are given by:

$$-\left(\tau_{zx} - \frac{\partial \tau_{zx}}{\partial z}\frac{1}{2}\delta z\right)\delta x\delta y + \left(\tau_{zx} + \frac{\partial \tau_{zx}}{\partial z}\frac{1}{2}\delta z\right)\delta x\delta y = \frac{\partial \tau_{zx}}{\partial z}\delta x\delta y\delta z \tag{3-11}$$

Thus, the total force per unit volume on the fulid due to the surface stresses is the sum of the force components which are expressed in Equation (3-9), (3-10), and (3-11):

$$\frac{\partial(-p + \tau_{xx})}{\partial x} + \frac{\partial \tau_{yx}}{\partial y} + \frac{\partial \tau_{zx}}{\partial z} \tag{3-12}$$

The momentum conservation equation in x, y, and z direction respectively can be expressed as follows:

$$\rho\frac{Du}{Dt} = \frac{\partial(-p + \tau_{xx})}{\partial x} + \frac{\partial \tau_{yx}}{\partial y} + \frac{\partial \tau_{zx}}{\partial z} + S_{Mx} \tag{3-13}$$

$$\rho\frac{Dv}{Dt} = \frac{\partial \tau_{xy}}{\partial x} + \frac{\partial(-p + \tau_{yy})}{\partial y} + \frac{\partial \tau_{zy}}{\partial z} + S_{My} \tag{3-14}$$

$$\rho \frac{Dw}{Dt} = \frac{\partial \tau_{xz}}{\partial x} + \frac{\partial \tau_{yz}}{\partial y} + \frac{\partial(-p + \tau_{zz})}{\partial z} + S_{Mz} \tag{3-15}$$

The souurce, $S_M$ is determined as the contribution to the body force per unit volume in the fluid.

### 3.2.3. Navier-Stokes equations for incompressible, isothermal flow

The derivation of the Navier-Stokes equation for incompressible, isothermal flow which is explained in this section is referring to Cengel & Cimbala (2014). For Fluid flow which is assumed to be both incompressible and isothermal, its pressure (p), dynamic viscosity (μ), and kinematic viscosity (ν) are set to be constant. Hence, it can be shown that the viscous stress tensor becomes:

$$\tau_{ij} = 2\mu\varepsilon_{ij} \tag{3-16}$$

Where $\varepsilon_{ij}$ = strain rate tensor. The viscous stress tensor in Equation (3-16) can be written into nine components in Cartesian coordinates and only six of which are independent due to symmetry:

$$\tau_{ij} = \begin{pmatrix} \tau_{xx} & \tau_{xy} & \tau_{xz} \\ \tau_{yx} & \tau_{yy} & \tau_{yz} \\ \tau_{zx} & \tau_{zy} & \tau_{zz} \end{pmatrix} = \begin{pmatrix} 2\mu\frac{\partial u}{\partial x} & \mu\left(\frac{\partial u}{\partial y} + \frac{\partial v}{\partial x}\right) & \mu\left(\frac{\partial u}{\partial z} + \frac{\partial w}{\partial x}\right) \\ \mu\left(\frac{\partial v}{\partial x} + \frac{\partial u}{\partial y}\right) & 2\mu\frac{\partial v}{\partial y} & \mu\left(\frac{\partial v}{\partial z} + \frac{\partial w}{\partial y}\right) \\ \mu\left(\frac{\partial w}{\partial x} + \frac{\partial u}{\partial z}\right) & \mu\left(\frac{\partial w}{\partial y} + \frac{\partial v}{\partial z}\right) & 2\mu\frac{\partial w}{\partial z} \end{pmatrix} \tag{3-17}$$

The stress tensor in Cartesian coordinates is written as:

$$\sigma_{ij} = \begin{pmatrix} -P & 0 & 0 \\ 0 & -P & 0 \\ 0 & 0 & -P \end{pmatrix} + \begin{pmatrix} 2\mu\frac{\partial u}{\partial x} & \mu\left(\frac{\partial u}{\partial y} + \frac{\partial v}{\partial x}\right) & \mu\left(\frac{\partial u}{\partial z} + \frac{\partial w}{\partial x}\right) \\ \mu\left(\frac{\partial v}{\partial x} + \frac{\partial u}{\partial y}\right) & 2\mu\frac{\partial v}{\partial y} & \mu\left(\frac{\partial v}{\partial z} + \frac{\partial w}{\partial y}\right) \\ \mu\left(\frac{\partial w}{\partial x} + \frac{\partial u}{\partial z}\right) & \mu\left(\frac{\partial w}{\partial y} + \frac{\partial v}{\partial z}\right) & 2\mu\frac{\partial w}{\partial z} \end{pmatrix} \tag{3-18}$$

Then, the Equation (3-18) is replaced into the three components of Cauchy's Equation. For the x-component, the equation becomes:

$$\rho \frac{Du}{Dt} = -\frac{\partial P}{\partial x} + \rho g_x + 2\mu\frac{\partial^2 u}{\partial x^2} + \mu\frac{\partial}{\partial y}\left(\frac{\partial v}{\partial x} + \frac{\partial u}{\partial y}\right) + \mu\frac{\partial}{\partial z}\left(\frac{\partial w}{\partial x} + \frac{\partial u}{\partial z}\right) \tag{3-19}$$

The Equation (3-19) can be arranged as:

$$\rho \frac{Du}{Dt} = -\frac{\partial P}{\partial x} + \rho g_x + \mu \left| \frac{\partial^2 u}{\partial x^2} + \frac{\partial}{\partial x}\frac{\partial u}{\partial x} + \frac{\partial}{\partial x}\frac{\partial v}{\partial y} + \frac{\partial^2 u}{\partial y^2} + \frac{\partial}{\partial x}\frac{\partial w}{\partial z} + \frac{\partial^2 u}{\partial z^2} \right|$$

$$= -\frac{\partial P}{\partial x} + \rho g_x + \mu \left[ \frac{\partial}{\partial x}\left(\frac{\partial u}{\partial x} + \frac{\partial v}{\partial y} + \frac{\partial w}{\partial z}\right) + \frac{\partial^2 u}{\partial x^2} + \frac{\partial^2 u}{\partial y^2} + \frac{\partial^2 u}{\partial z^2} \right]$$

(3-20)

The last three terms in Equation (3-20) is the Laplacian of velocity component u. Therefore, the momentum equation in the x-, y-, z- component can be written as:

$$\rho \frac{Du}{Dt} = -\frac{\partial P}{\partial x} + \rho g_x + \mu \nabla^2 u \tag{3-21}$$

$$\rho \frac{Dv}{Dt} = -\frac{\partial P}{\partial y} + \rho g_y + \mu \nabla^2 v \tag{3-22}$$

$$\rho \frac{Dw}{Dt} = -\frac{\partial P}{\partial z} + \rho g_z + \mu \nabla^2 w \tag{3-23}$$

Those three components can be combined into one vector equation: The Navier-Stokes equation for incompressible flow with constant viscosity (Equation (3-24))

$$\rho \frac{D\vec{V}}{Dt} = -\vec{\nabla}P + \rho \vec{g} + \mu \nabla^2 \vec{V} \tag{3-24}$$

The continuity and Navier-Stokes Equations in cylindrical coordinates can be expressed as follows:

- Incompressible continuity equation:

$$\frac{1}{r}\frac{\partial (r u_r)}{\partial r} + \frac{1}{r}\frac{\partial (u_\theta)}{\partial \theta} + \frac{\partial (u_z)}{\partial z} = 0 \tag{3-25}$$

- r-component of the incompressible Navier-Stokes equation:

$$\rho \left( \frac{\partial u_r}{\partial t} + u_r \frac{\partial u_r}{\partial r} + \frac{u_\theta}{r}\frac{\partial u_r}{\partial \theta} - \frac{u_\theta^2}{r} + u_z \frac{\partial u_r}{\partial z} \right)$$

(3-26)

$$= -\frac{\partial P}{\partial r} + \rho g_r + \mu \left[ \frac{1}{r}\frac{\partial}{\partial r}\left(r\frac{\partial u_r}{\partial r}\right) - \frac{u_r}{r^2} + \frac{1}{r^2}\frac{\partial^2 u_r}{\partial \theta^2} - \frac{2}{r^2}\frac{\partial u_\theta}{\partial \theta} + \frac{\partial^2 u_r}{\partial z^2} \right]$$

- $\theta$-component of the incompressible Navier-Stokes equation:

$$\rho \left( \frac{\partial u_\theta}{\partial t} + u_r \frac{\partial u_\theta}{\partial r} + \frac{u_\theta}{r} \frac{\partial u_\theta}{\partial \theta} + \frac{u_r u_\theta}{r} + u_z \frac{\partial u_\theta}{\partial z} \right) \tag{3-27}$$
$$= -\frac{1}{r} \frac{\partial P}{\partial \theta} + \rho g_\theta + \mu \left[ \frac{1}{r} \frac{\partial}{\partial r} \left( r \frac{\partial u_\theta}{\partial r} \right) - \frac{u_\theta}{r^2} + \frac{1}{r^2} \frac{\partial^2 u_\theta}{\partial \theta^2} + \frac{2}{r^2} \frac{\partial u_r}{\partial \theta} + \frac{\partial^2 u_\theta}{\partial z^2} \right]$$

- z-component of the incompressible Navier-Stokes equation:

$$\rho \left( \frac{\partial u_z}{\partial t} + u_r \frac{\partial u_z}{\partial r} + \frac{u_\theta}{r} \frac{\partial u_z}{\partial \theta} + u_z \frac{\partial u_z}{\partial z} \right) \tag{3-28}$$
$$= -\frac{\partial P}{\partial z} + \rho g_z + \mu \left[ \frac{1}{r} \frac{\partial}{\partial r} \left( r \frac{\partial u_z}{\partial r} \right) + \frac{1}{r^2} \frac{\partial^2 u_z}{\partial \theta^2} + \frac{\partial^2 u_z}{\partial z^2} \right]$$

## 3.3.    Introduction to OpenFOAM

This thesis is utilizing OpenFOAM to simulate and study flow inside the pipe. According to Wikipedia (2016), OpenFOAM which stands for Open Source Field Operation and Manipulation, is the open source CFD software. It is under the GNU General Public License and it is managed, maintained, and distributed by the OpenFOAM Foundation. This computational program is used in the "solver" stage in CFD. OpenFOAM is written in C++ program and it is commonly compatible in Unix/Linux operating systems.

There are several advantages of this computational program according to CFD support (2016). First, it is capable to generate individualized solutions. Different from any other commercial software, the great extent of custom development is provided by OpenFOAM. Thus, OpenFOAM suits for any unique and specific cases of fluid flow. Second, OpenFOAM requires no licenses for unlimited number of users. Thus, it is completely free of charge. Third, OpenFOAM is able to execute much more accurate results in a short time frame, compared to the results which are obtained by experimentation in the laboratory.

Apart from its interesting features, the OpenFOAM toolbox also has some weaknesses. According to Lysenko et al. (n.d), the OpenFOAM has limitation in the default settings, non-existence in the quality certification, lack of high-quality documentation and references. It produces an impression that any kind of problem can be solved since it contains large amount of different numerical schemes, algorithms, and mathematical models. In addition, the use of the mathematical model for solving complex problems has not yet been evaluated. The limitations of application of the most of the models are also not well recognized.

Therefore, the most crucial problem of any numerical investigation is to estimate the capabilities of the numerical simulations.

### 3.3.1. Courant number

According to Singh (1996), the Courant Number is a value to determine the amount of flow moves in a computational grid cell in a given time-step. In this case, for the explicit Eulerian method, the Courant number shall not be greater than one. When the Courant number exceeds one, it indicates that the flow passes on the more than one grid at each time step. As the result, the time-integrator has no chance to translate the occurred physics accurately. Therefore, the results will not be stable and the extreme impact is it will damage the model. The Courant number in one-dimension is expressed as:

$$C \equiv \frac{u\,\Delta t}{\Delta x} \tag{3-29}$$

Where u = characteristic flow speed of the system, $\Delta t$ = time-step of the numerical model, and $\Delta x$ = spacing of the grid in the numerical model.

# Chapter 4.  Numerical Set-up

## 4.1.    Geometry model

The geometry models, which are studied in this thesis consist of straight pipes, blind-tee pipes, and elbow pipes. Each of these models have diameter (D) of 1 m. The length of the straight pipe equals to ten times diameter (L = 10D). While, the length of blind-tee pipe varies from 1D to 5D. The studied elbow pipe has an outside radius (A) of 0.5D. In Figure 4.2 it shows that one of the blind-tee pipe model with a blind-tee length equals to 5D. While, Figure 4.1 and Figure 4.3 exhibits the geometry model of straight pipe and elbow pipe, respectively.
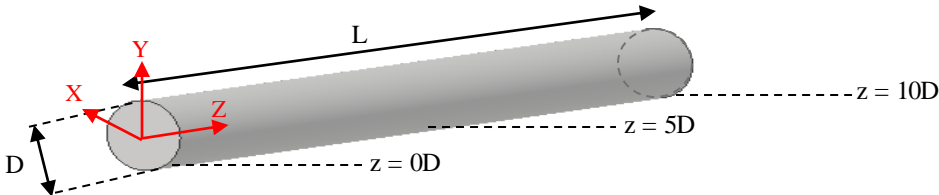


**Figure 4.1.** Geometry Model of Straight Pipe
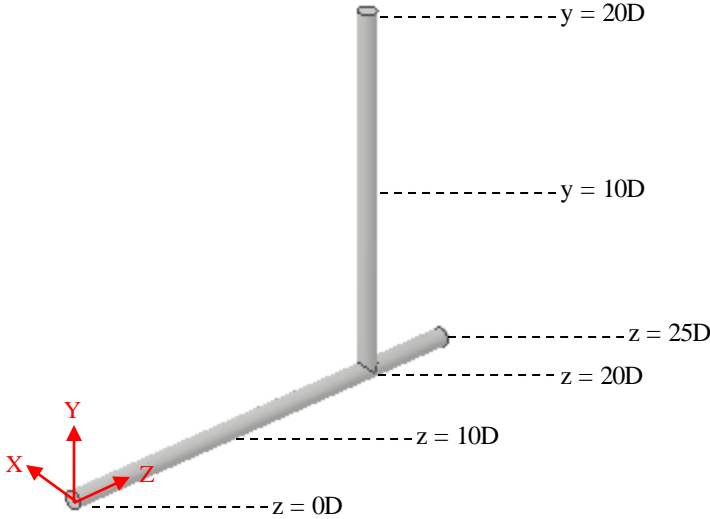


**Figure 4.2.** Geometry Model of Blind-tee Pipe with the Tee Length = 5D

26
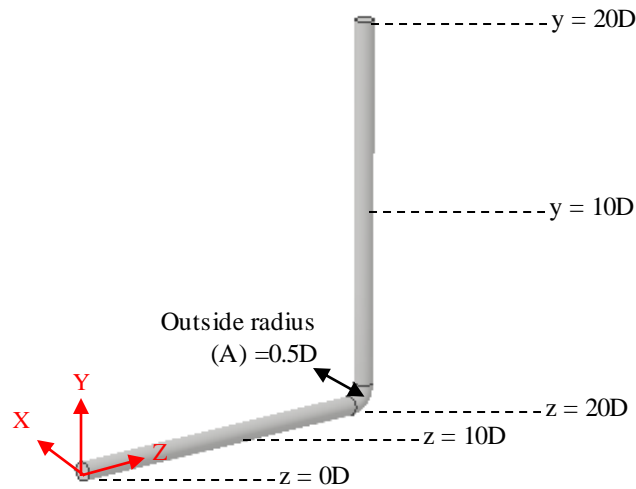
**Figure 4.3.** Geometry Model of Elbow Pipe

## 4.2. Meshing

According to CFD-Online (2012), the fluid flow in CFD simulation shall be analyzed correctly and properly in order to obtain the accurate solutions. The governed partial differential equations for the complex fluid flow cases usually cannot be manageable easily by the analytical solutions. In the CFD simulation, the fluid flow domains have to be divided into smaller subdomains or elements/cells so that the governing equations can be solved inside every single of these subdomains. The mesh elements are classified based on the dimensions and type of elements. The selections of the type of elements are based on the problem and the competence of the solver. Figure 4.4 exhibits the elements type of the mesh.
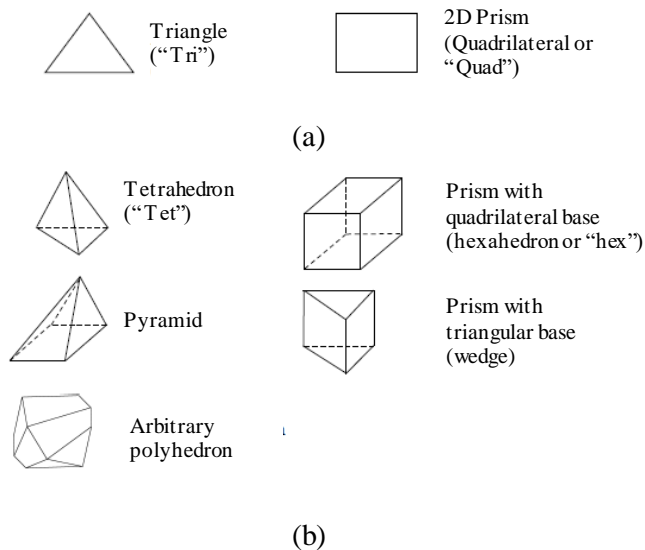


**Figure 4.4.** (a) 2-Dimensional Element Types, (b) 3-Dimensional Element Types (Bakker, 2006, p. 6)

There are three methods which can be utilized to solve the governed equations, such as finite volumes, finite elements, and finite differences. However, only one of them is used depending on the type of the elements. This method should be carried out carefully in order to make sure that the continuity of the solution across the interfaces of elements is done properly. Furthermore, the purpose is to obtain a complete picture of the fluid flow in the whole domain.

Besides the element type of the mesh, there is another mesh classification in CFD: the connectivity-based classification. This classification is the most basic form of the mesh classification (CFD-Online, 2007). It is known as:

- Structured Meshes
  The characteristic of this mesh is shown by the regular connectivity. The structured mesh can be indicated as two or three dimensional array. The selection of the mesh type is limited to quadrilaterals in 2-Dimensional or hexahedra in 3-Dimensional. The advantage of structured mesh is the ability to save space since the relationships of each elements/cells are determined by the storage arrangement.

- Unstructured Meshes
  This mesh is characterized by the irregular connectivity. Moreover, it is not easily demonstrated as a two or three dimensional array. Hence, it permits any conceivable elements that solver may be able to utilize.

In generating mesh, the high quality of mesh should be achieved since the poor quality of mesh is causing the inaccurate solution and convergence. There are three assessments of mesh quality according to Bakker (2006):

1) Skewness
   Skewness defines the ideal of an element of cell. Basically, the governing equations which are solved in the CFD, have the assumption that the elements are relatively equilateral or equiangular (see Figure 4.5). Therefore, the mesh which is highly skewed will lead to an inaccurate solution. According to Bakker (2006), the recommended element/cell skewness of Hexahedron and quadrilateral cells is < 0.85. For triangualar and tetrahedron cells, the recommended cells skewness are less than 0.85 and 0.9, respectiveley.
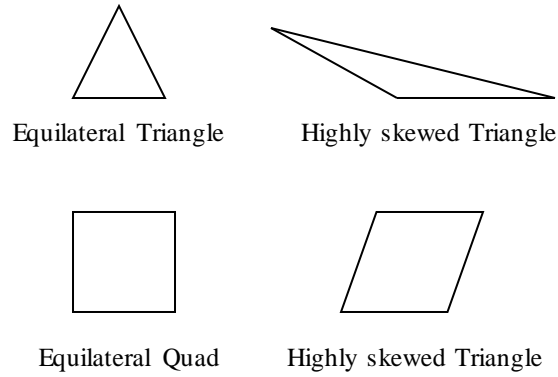
**Figure 4.5.** The Ideal and Highly Skewed Elements of Mesh (WIKI2, 2015)

2) Smoothness and aspect ratio

The change of the element size shall not be to significant in order to avoid the discontinuity of solving the governing equations between elements/cells. The smooth and sudden change of mesh elements are illustrated in Figure 4.6.
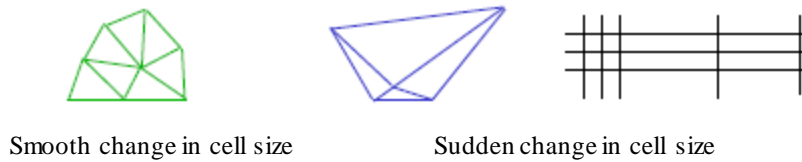


**Figure 4.6.** The Example of Smooth and Sudden Change in Cell Size (Bakker, 2006, p. 26)

3) Aspect ratio

The aspect ratio is the ratio between the longest edge length and the shortest edge length. The ideal ratio is one for an equilateral triangle or a square as is shown in Figure 4.7.
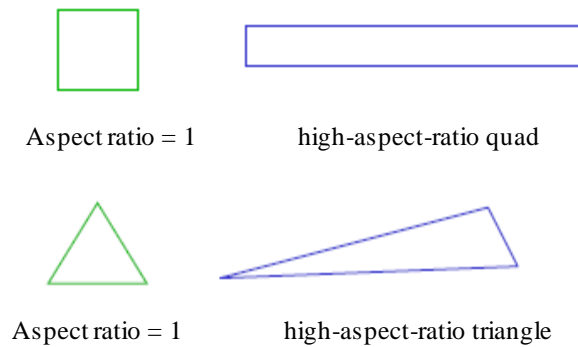


**Figure 4.7.** The Example of Ideal and High Aspect Ratio Cells (Bakker, 2006, p. 26)

Bakker (2006) also explained the guidelines of generating a mesh in order to achieve a good quality of mesh. The description of those guidelines will be explained as follows:

1) Resolution

The elements where the particular flow occurs, shall be created adequetely. The ratio between the width and the heigh of a cell shall be near one where the flow is multi-dimensional (e.i. x, y, z direction). When the flow is fully developed and mainly in one-dimensional, the quad/hex cells can be stretched in order to avoid very high number of mesh elements. Figure 4.8 exhibits the example of mesh resolutions.



(a)



(b)
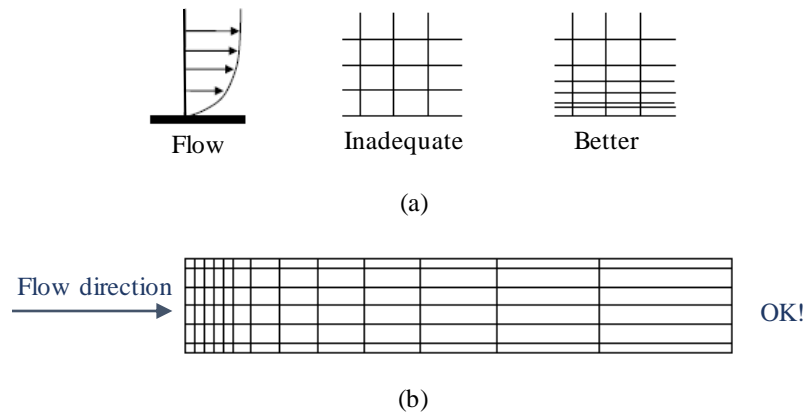
**Figure 4.8.** The Example of Mesh Element Resolution for: (a) Near Wall Region and (b) Fully Developed Flow Region (Bakker, 2006, p. 28)

2) Smoothness

Another guideline to have a good mesh generation is a good transition of element size. The ideal of the maximum change in grid spacing shall be less than 20%. Figure 4.9 illustrates the definition of grid spacing between two elements/cells.



$$\frac{\Delta x_{i+1}}{\Delta x_i} \leq 1.2$$
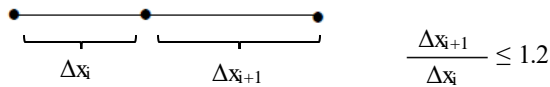
**Figure 4.9.** The Illustration of Grid Spacing of Two Elements (Bakker, 2006, p. 29)

3) Total cell count

Basically, the more cells or elements in the flow domains give the higher precision in solving the governing equation in the flow domain. However, the more elements in flow domain will increase the memory and CPU time. Therefore, to maintain the number of elements in the appropriate

number, the high mesh resolution can be used at the selected areas where it would require a more precise solution.

The mesh set up for the straight pipe case is explained in Chapter 5. Furthermore, for the blind-tee and elbow shape pipe case is described in Chapter 6.

## 4.3. Boundary condition

The boundary conditions shall be determined in order to provide information about the velocity fields and its gradient at the natural boundary of the flow domain. The information of the boundary conditions is used as additional statements for solving the governing equations for the velocity and pressure fields. It is understood that these governing equations are partial differential equations which are modeled as continuum that occurs in every point in the fluid. Therefore, when integrating them in specific situation, the arbitrary functions and/or constants can be expected.

The boundary condition of straight pipe, blind-tee pipe, and elbow pipe of this thesis are illustrated in Figure 4.10, 4.11, and 4.12, respectively:
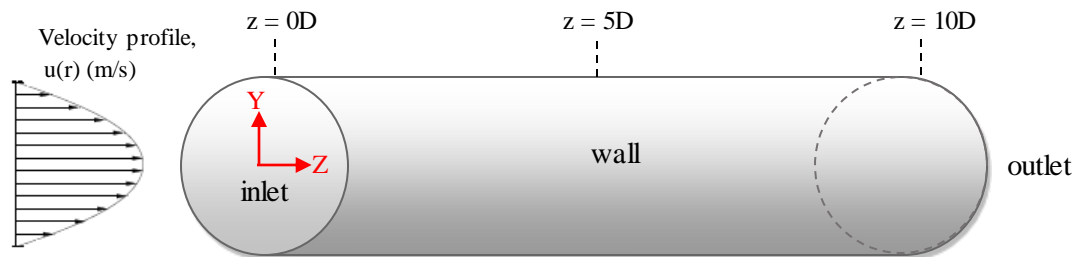


**Figure 4.10.** Schematic of Boundary Condition of Straight Pipe

outlet

wall

Y

inlet →Z          wall          wall     wall
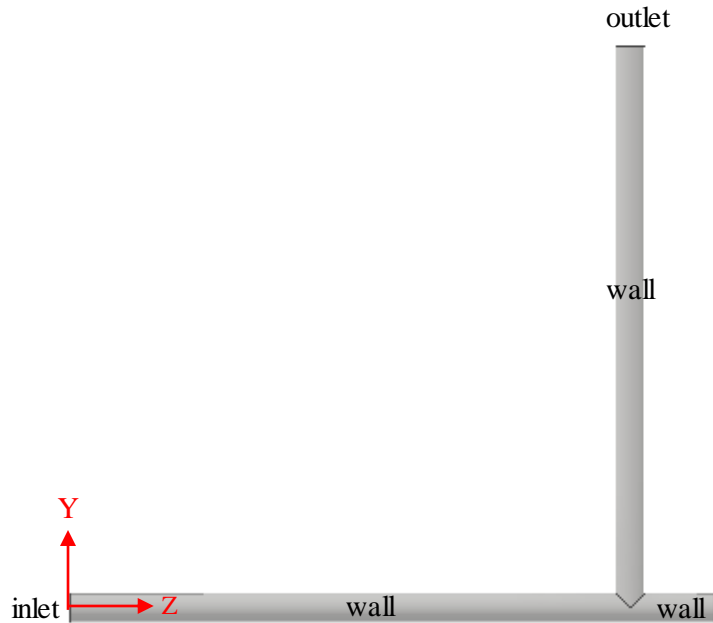
**Figure 4.11.** Schematic of Boundary Condition of Blind-tee Pipe

outlet

wall

Y

inlet →Z          wall
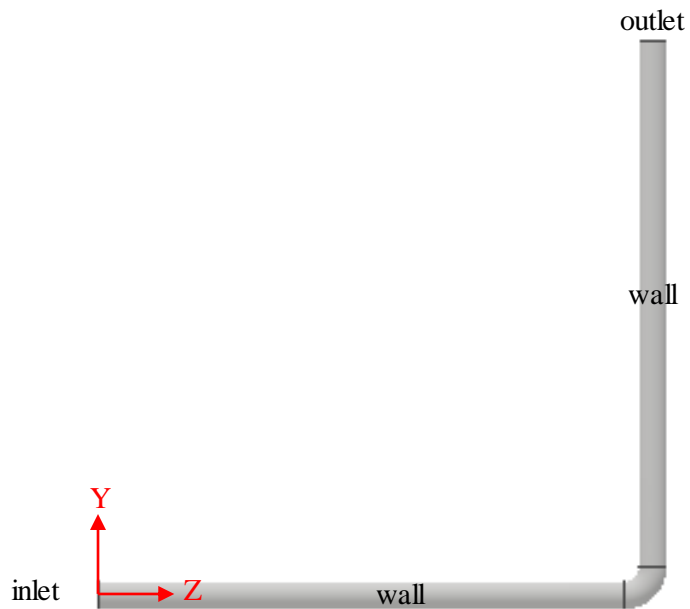
**Figure 4.12.** Schematic of Boundary Condition of Elbow Pipe

There are three boundary conditions for the straight pipe, blind-tee pipe, and elbow pipe which are explained as follows:

- **Inlet**

  At the inlet, in order to save simulation time of laminar flow simulation and to avoid using a very long pipe, a developed velocity profile with the initial average velocity equals to 1 m/s is generated analytically by using the classical formula (see Equation (2-13) for the detailed description).

  $$U_x = 0 \; ; \; U_y = 0 \; ; \; U_z = u(r); \tag{4-1}$$

  The pressure boundary conditions at the inlet are set to be zero gradient for every direction:

  $$\frac{\partial P}{\partial x} = 0 \; ; \; \frac{\partial P}{\partial y} = 0 \; ; \; \frac{\partial P}{\partial z} = 0 \tag{4-2}$$

- **Wall**

  At the wall, a non-slip condition is set for this boundary. Therefore, the velocity is set to zero for every direction and the pressure is set to be zero gradient for every direction:

  $$U_x = 0 \; ; \; U_y = 0 \; ; \; U_z = 0 \tag{4-3}$$

  $$\frac{\partial P}{\partial x} = 0 \; ; \; \frac{\partial P}{\partial y} = 0 \; ; \; \frac{\partial P}{\partial z} = 0 \tag{4-4}$$

- **Outlet**

  At the outlet, the velocity is set to be zero gradient for every direction and the pressure is set to be zero:

  $$\frac{\partial u}{\partial x} = 0 \; ; \; \frac{\partial v}{\partial y} = 0 \; ; \; \frac{\partial w}{\partial z} = 0 \tag{4-5}$$

  $$P_x = 0 \; ; \; P_y = 0 \; ; \; P_z = 0 \tag{4-6}$$

## 4.4. Solver set-up

The OpenFOAM solver which is employed in this thesis is pimpleFoam. According to OpenFOAM (2011), pimpleFoam is a large time-step transient solver which is suitable for incompressible, Newtonian, non-Newtonian, laminar, and turbulent flow. This solver uses the merged PISO-SIMPLE algorithm which is known as PIMPLE algortihm. The PISO algorithm (Pressure Implicit with Splitting of Operators) is the calculation procedure for generating the pressure-velocity which is initially for non-iterative computation of unsteady compressible flows. Then, this algorithm has been modified to solve the iterative soution of

steady state problems (Versteeg & Malalasekera, 1995). While the SIMPLE algorithm which stands for Semi-Implicit Method for Pressure Linked Equations, generates the pressure from velocity components by utlizing the Navier-Stkoes equations combined with iterative procedure (Ferziger & Peric, 1999).

In order to specify a turbulence models in OpenFoam solver, the keyword of simulationType shall be given. Since laminar flow is modeled in the present study, "laminar" is employed as the keyword for the simulationType. The kinematic viscosity is specified in the tranportProperties input file. In addition, the "Newtonian" keyword shall be applied as the keyword for the transportModel. The fluid simulated in the present study is Newtonian and Incompressible fluid.

The discretisation scheme for this solver is in accordance with Greenshields (2011). The discretisation scheme set up for the first time derivative $(\partial/\partial t)$ terms is Euler which is an implicit, bounded scheme that has first order accuracy. For the gradient schemes, Gauss is set as the discretization method with linear interpolation. The discretization scheme Gauss means gaussian integration with second order. In the divergence scheme, bounded Gauss is set as the discretization scheme and linearUpWind as the interpolation scheme. For the Laplacian schemes, the discretization method for all variable is Gauss with a linear interpolation. In addition, the scheme is set to be corrected which is unbounded, second order, and conservative numerical behaviour. The interpolation scheme which is the shceme method of data interporlation is set as linear and specified as default. The input files for the discretisation scheme is presented in Appendix D.

# Chapter 5.   Straight Pipe Case

## 5.1.   Introduction

According to Wermac (2008), a pipe is explained as a hollow tube that has round cross section which is used to transport some products, such as fluids, gas, pellets, powders, and more. The straight pipe which is studied in this thesis is required to be installed at the upstream and donwstream of the pipe fittings or pipe joints in order to obtain a fully developed desirable flow profile.

## 5.2.   Methodology

This thesis starts from studying the flow inside the straight pipe in order to obtain the correct velocity profile before studying pipes with other geometries. In this section, the procedure of analyzing the straight pipe analysis will be discussed.

The analysis of straight pipe case will be divided into two geometries: 2-Dimensional (2-D) geometry and 3-Dimensional (3-D) geometry. This thesis starts from the analysis of 2-D geometry. In the first stage, the 2-D geometry and its mesh are created. Moreover, its boundary condition is set as well. After the geometry is sketched, the next step is to perform the laminar flow analysis with PimpleFoam solver. Then, the result from this numerical solution will be validated with the analytical solution obtained from a classical formula (see Equation (2-13)). In the post-processing stage, the velocity profile is plotted, and the 3-D geometry analysis can be proceeded.

After the mesh and the geometry of the 3-D geometry have been set properly, the next step is carrying out the laminar flow analysis with PimpleFoam solver. Then, after the velocity profile is converged and fitted with the analytical solution of the classical formula, the velocity profile can be plotted.

Figure 5.1 shows the procedure chart for the straight pipe case:
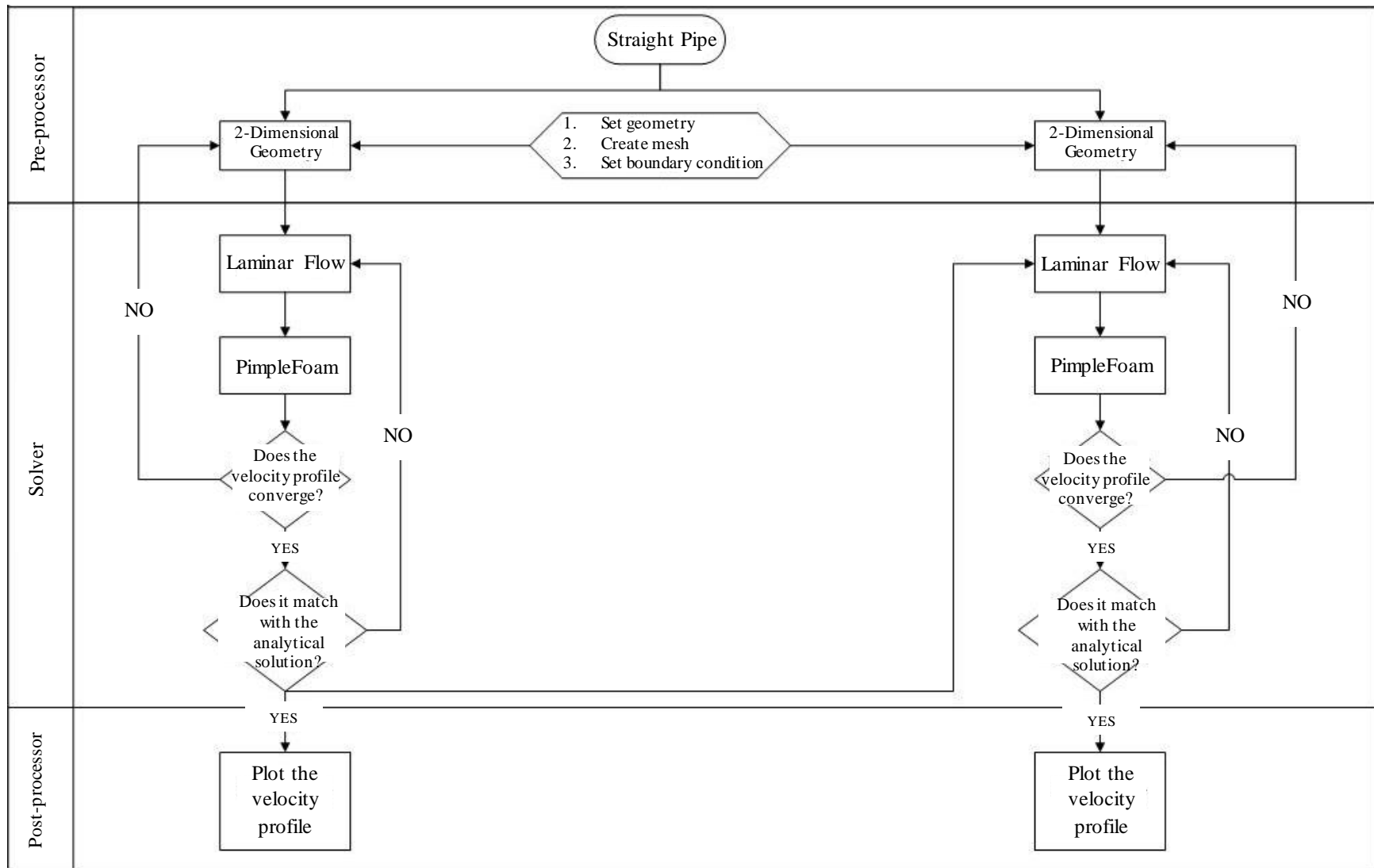
**Figure 5.1.** The Procedure of Straight Pipe Case

## 5.3.   Mesh set-up

Good and correct meshing needs to be done in order to achieve an accurate CFD result by using the OpenFOAM. The mesh set-up is the crucial part for the CFD simulation. This stage takes 60% of the project time in order to achieve the correct meshing geometry. Therefore, a good result of the velocity profile can be obtained. GMSH software is used for setting up the mesh for the straight pipe case.

Structured mesh is used for the straight pipe 2-D cases. However, for 3-D cases, structured mesh is used for flow region near to the pipe wall, whereas unstructured mesh is used at the region where the flow is fully developed (the center of the pipe). The aim is to avoid the huge amount of mesh elements and maintain a good quality of mesh. The correct mesh set-up for the geometry of straight pipe case is shown in Figure 5.2.
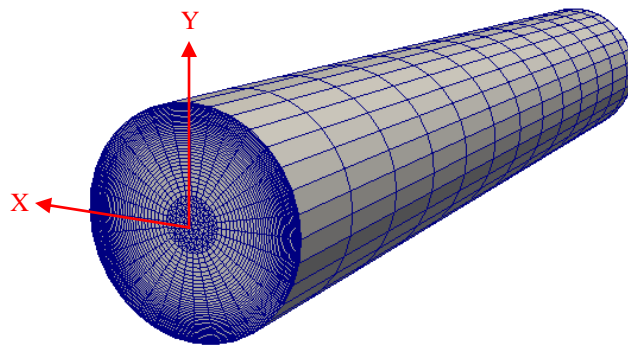


**Figure 5.2.** Mesh Set-up of the Straight Pipe Case

Figure 5.3 exhibits the correct and incorrect mesh set-up. The differences can be recognized clearly from those figures. In the Figure 5.3(a), the correct mesh set-up shows good resolution of the fine meshing at pipe wall. Moreover, the size of the mesh element increases smoothly towards the center of the pipe. However, the incorrect mesh-set up as shown in Figure 5.3(b) is sketched in the opposite way which the center of the pipe is set to be very fine and progressively coarse towards the pipe wall. These methods of constructing the mesh indeed give significant impact to the result of the velocity profile as shown in the Figure 5.4.

(a)                                                                                    (b)
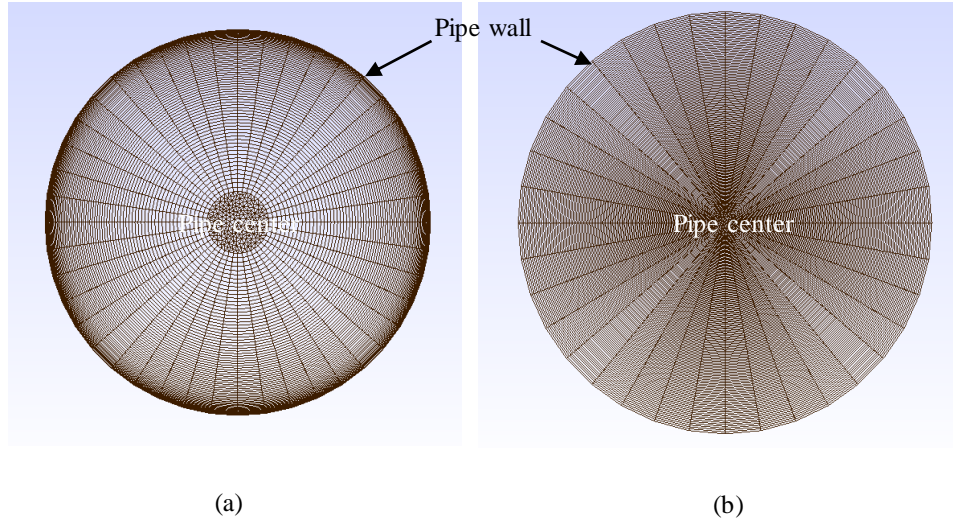
**Figure 5.3.** The Visualization of: (a) Correct Mesh Set-up for 3-Dimensional Geometry Cross-section; (b) Incorrect Mesh Set-up for 3-Dimensional Geometry Cross-section
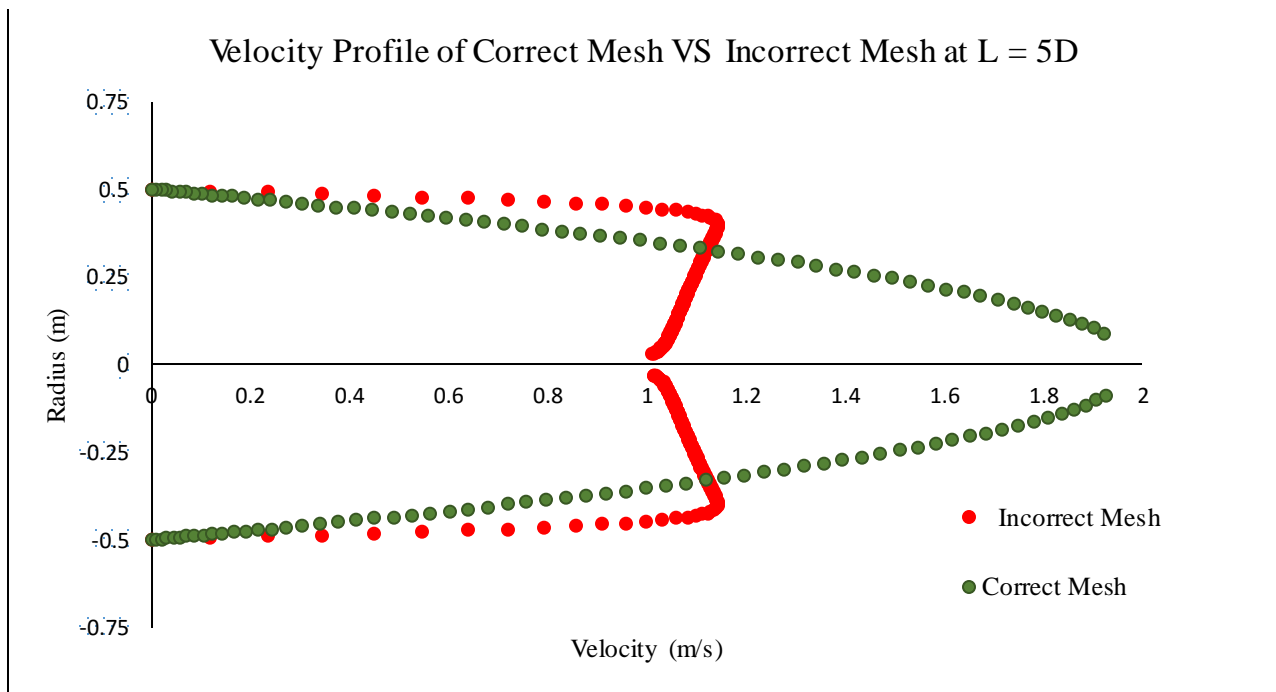


**Figure 5.4.** The Velocity Profile of Correct Vs Incorrect Mesh Set-up

## 5.4. Sensitivity study

The aim of sensitivity study which is carried out in this thesis is to identify how the different values of various independent parameters such as mesh elements, time-steps, and Reynolds number will affect the velocity profile under given sets of simulated conditions. Before studying complex 3-D geometry (e.g. straight pipe, blind-tee pipe, and elbow pipe), it is better to start from the simple geometry with the simple analysis of 2-D simulation. The objective of this work is to have a good control of the geometry and mesh.

As it can be seen from the flow chart diagram of methodology (see Figure 5.1), the first step is to carry out the 2-D simulation of laminar pipe flow. The 2-D pipe geometry has 10 m length and 0.5 m distance from the wall. The pimpleFoam solver with the time step ($\Delta T$) = 0.01 s and Reynold number (Re) = 500 is used for the convergence study of different mesh elements: 16,744, 33,787, and 50,232. Moreover, the velocity profile which is obtained analytically by using the classical formula is used as the inlet velocity. Before the simulation is performed, the mesh of the geometry should be made to be sufficient enough to capture the flow along the pipe. The explanation of how to create proper mesh has been done in the Section 4.2. The result of the convergence study in different mesh elements is presented in Figure 5.5 and Table 5.1.
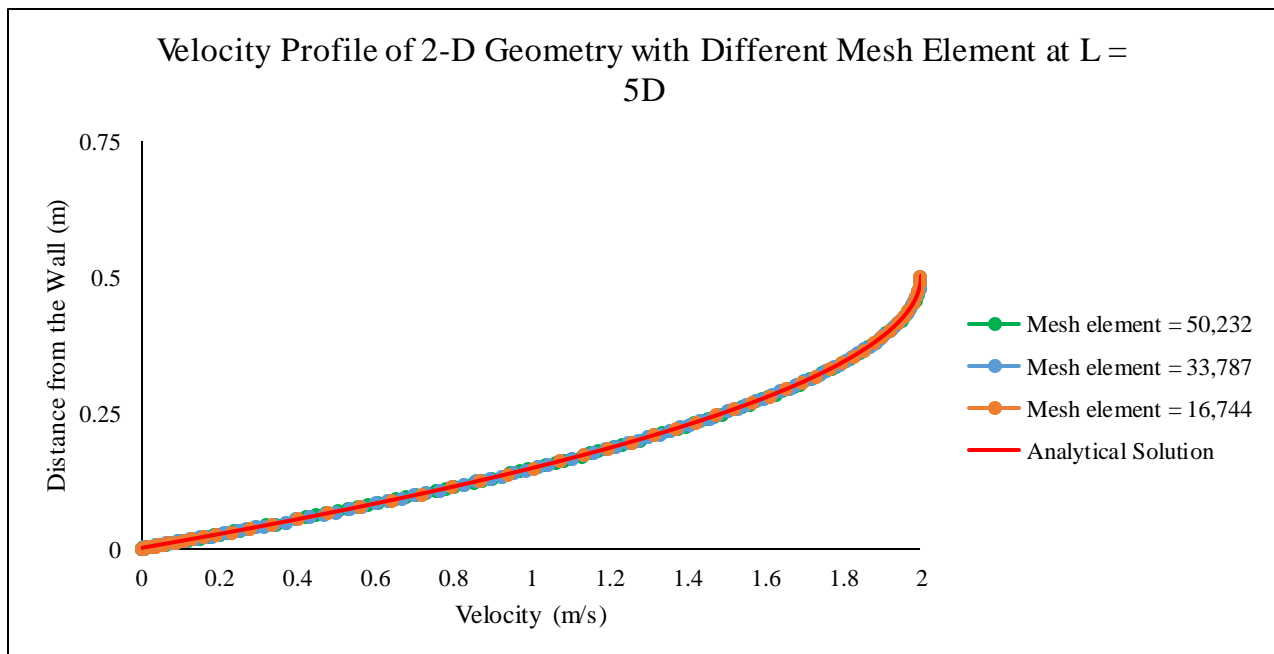


**Figure 5.5.** The Velocity Profile of 2-Dimensional Geometry with Different Element of Mesh

**Table 5.1.** The List of Courant Number of Different Mesh Element.

| Mesh Element | Courant Number |
|---|---|
| 16,744 | 0.2 |
| 33,787 | 0.2 |
| 50,232 | 0.2 |

The Figure 5.5 exhibits the comparison of the different mesh element at Re = 500. As it shown in the figure, the velocity profiles of the different mesh elements are the same. Based on this result, for the laminar flow analysis, the number of elements do not have significant impact to the velocity profile. Figure 5.6 presents the velocity profile along the pipe with 16,744 mesh elements and Re = 500.
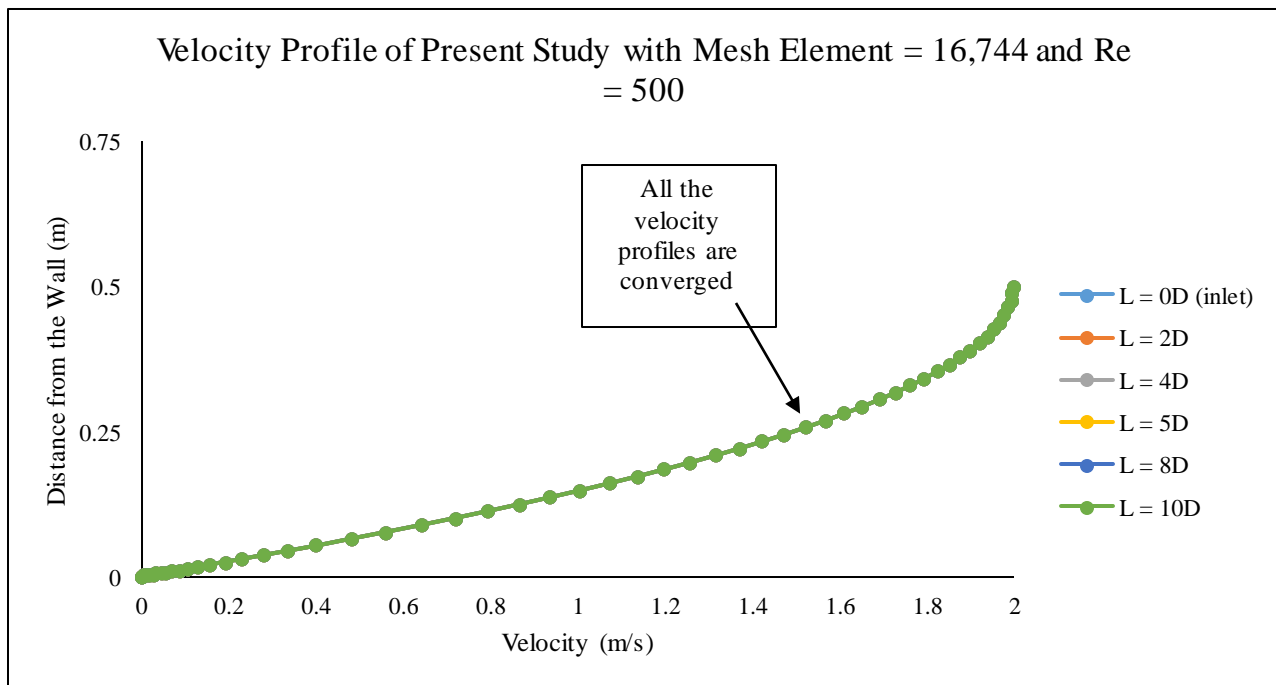


**Figure 5.6.** The Velocity Profile of 2-Dimensional Geometry Derived from PimpleFoam Solver

As it can be seen in Figure 5.6, the velocity profiles along the pipe (L = 0D, 2D, 4D, 5D, 8D, and 10D) show a good convergence and the flow is fully developed along the pipe. The courant number is 0.2 with time step, $\Delta T = 0.01$ s. This courant number meets the requirement of less than 1 (Thaker & J., 2011).

In order to see how sensitive the results of this simulation towards different Reynolds number are, the next analysis is to study the 2-D geometry in the different Reynolds number of 500, 1000, and 2000, with the mesh element of 16,744. In the input file of the pimpleFoam solver, the kinematic viscosity (ν) shall be adjusted in order to achieve the targeted Reynolds number. The Reynolds number which is used are presented in Table 5.2. The results of the velocity profile is shown in Figure 5.7, 5.8, and 5.9.

**Table 5.2.** Reynolds Number and Kinematic Viscosity Based on Average Velocity of 1m/s and Radius of 0.5 m

| Reynolds Number | Kinematic viscosity, ν (m²/s) |
|:---:|:---:|
| 500 | $1 \times 10^{-3}$ |
| 1000 | $5 \times 10^{-4}$ |
| 2000 | $2.5 \times 10^{-4}$ |
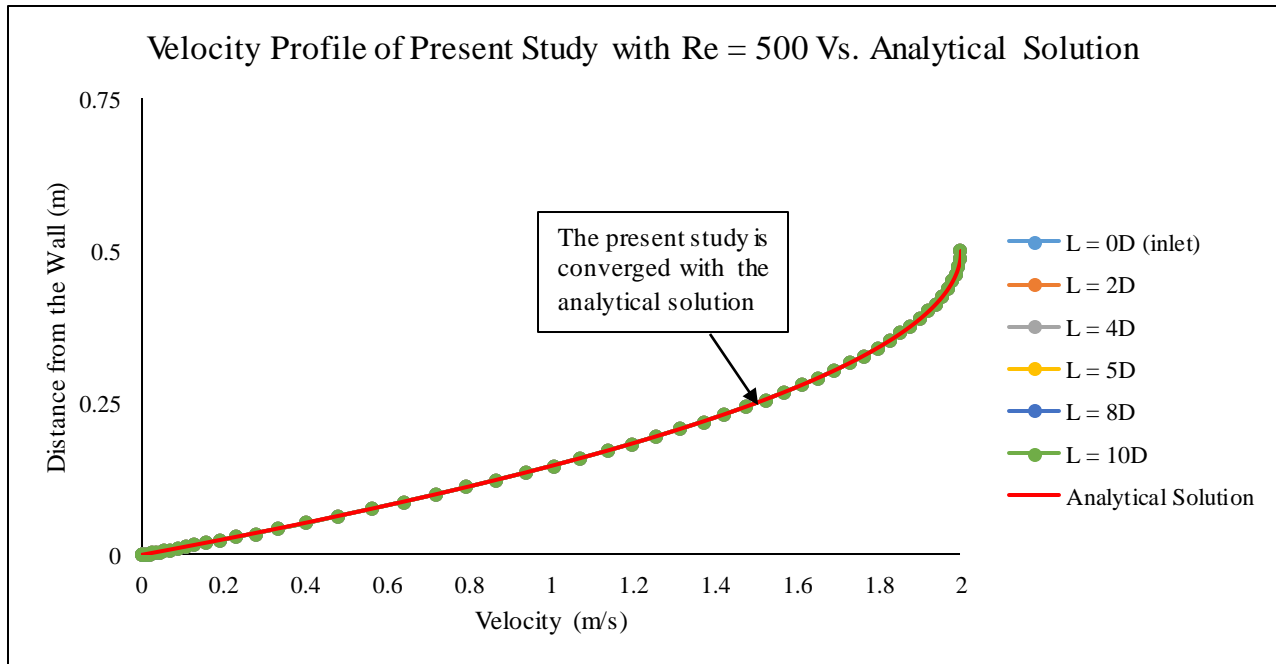


**Figure 5.7.** Velocity Profile of Present Study with Re = 500 Vs. Analytical Solution
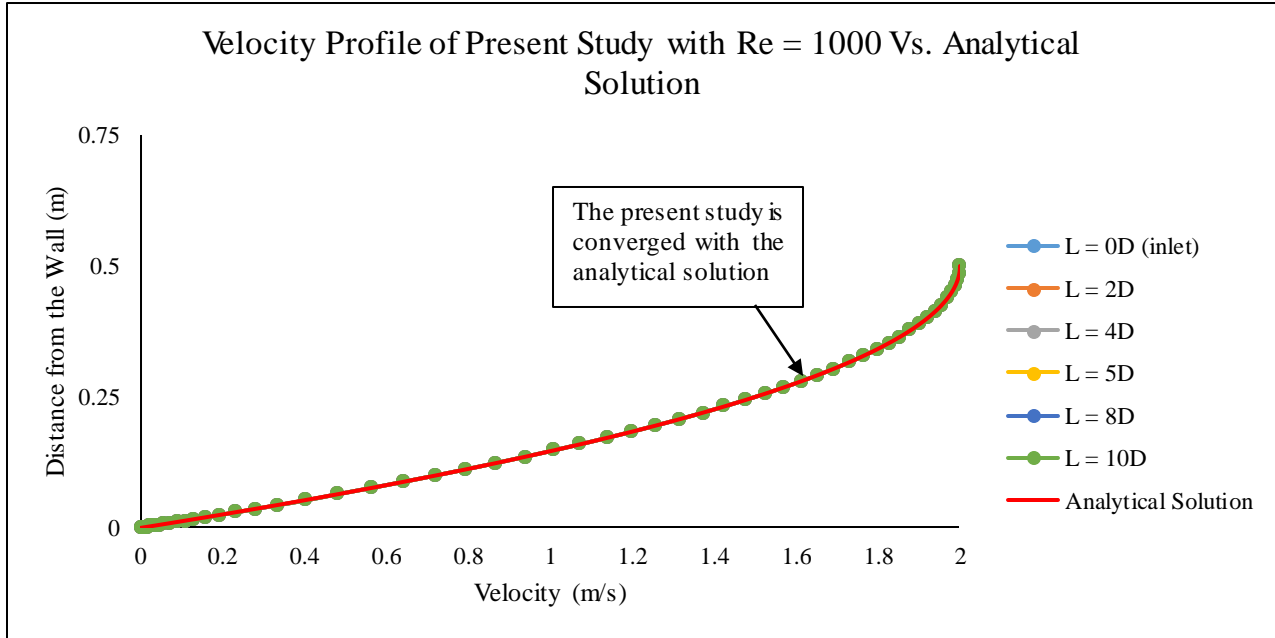
**Figure 5.8.** Velocity Profile of Present Study with Re = 1000 Vs. Analytical Solution
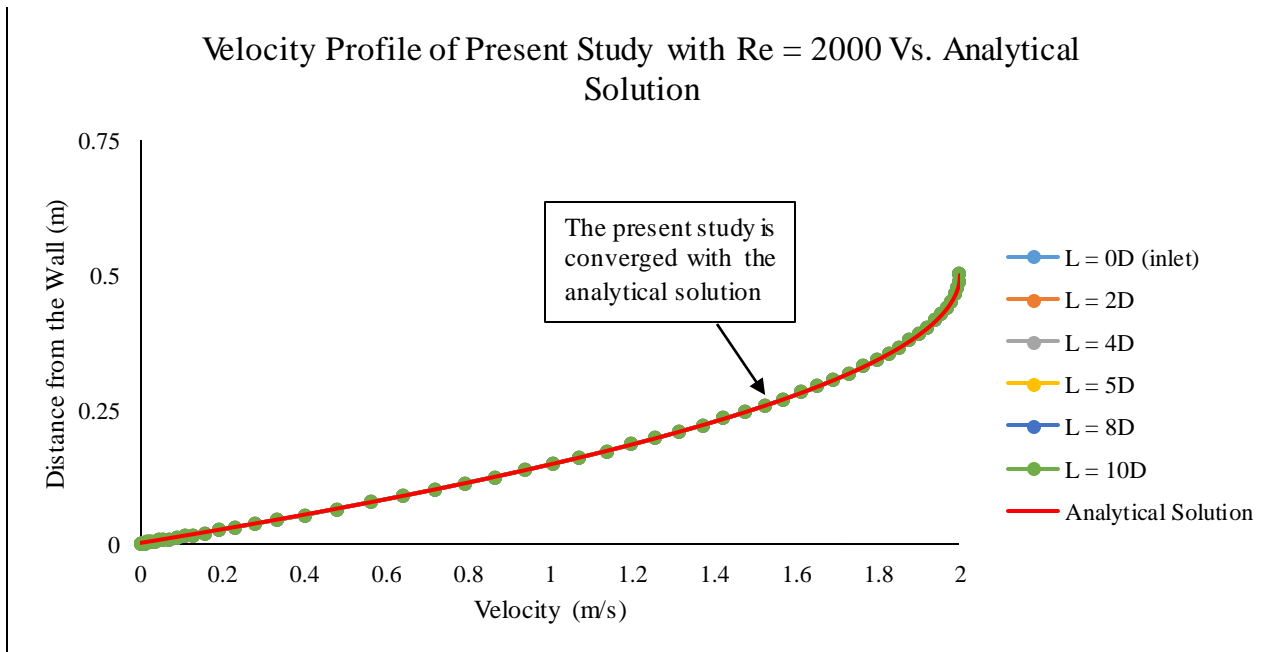


**Figure 5.9.** Velocity Profile of Present Study with Re = 2000 Vs. Analytical Solution

The Figure 5.7, 5.8, and 5.9 shows the comparison of the velocity profile obtained from analytical solution and the present study. The present numerical results are in agreement with the prediction achieved from the analytical solution.

42

## 5.5.  Validation study

After performing the laminar flow analysis for 2-D geometry, the next step is to execute the laminar flow analysis for 3-D simulation. From the previous simulation, the pimpleFoam solver has been proved to be suitable for the laminar flow analysis. Thus, in the 3-D geometry analysis, the same solver as in the 2-D simulation analysis will be used.

Before proceeding the simulation, the geometry and the mesh shall be established correctly. In addition, the boundary condition shall be applied properly as well. The 3-D geometry has a diameter (D) of 1 m and pipe length (L) of 10D. The first simulation is to perform the laminar flow analysis with different mesh elements. The purpose of this simulation is to study the sensitivity of mesh towards the low Reynolds number (Re = 1000). The result can be seen in the Figure 5.10.
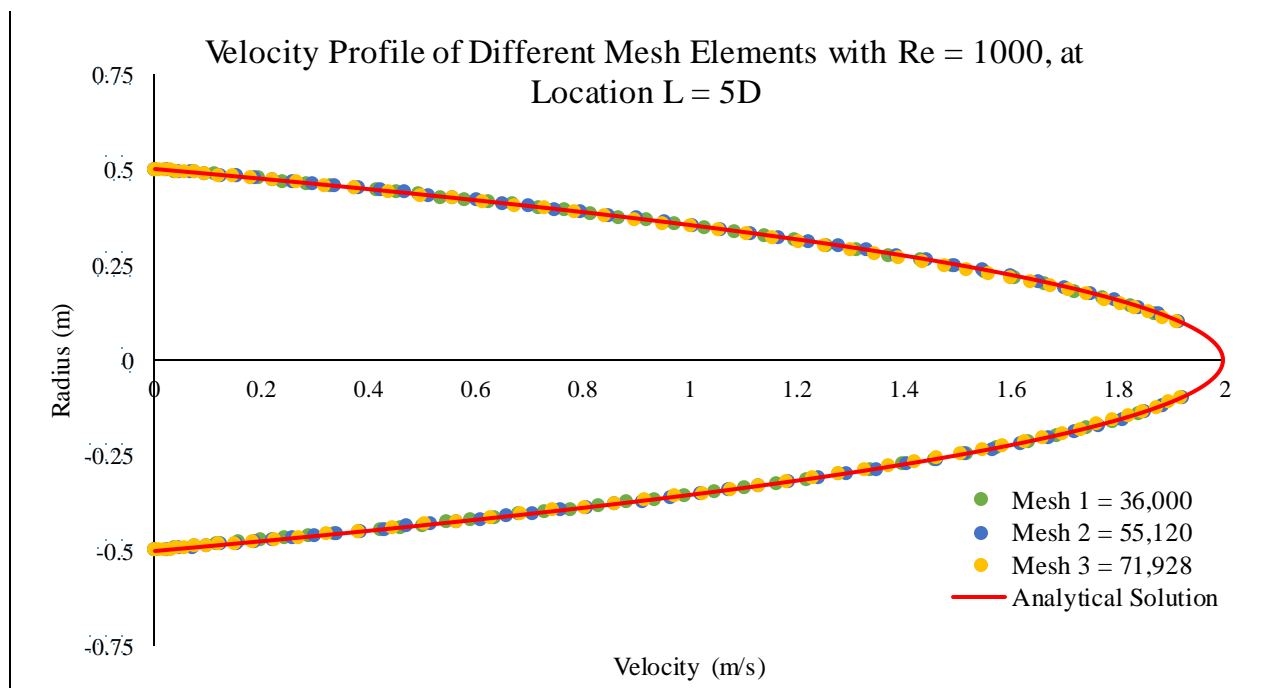
**Figure 5.10.** The Velocity Profile of 3-Dimensional Geometry with Different Mesh Elements at Location: L = 5D with Re = 1000

Figure 5.10 shows the result of the velocity profiles from the 3-D geometry which has mesh elements of 36,000, 55,120, and 71,928. These three mesh elements almost give the same velocity profiles at L = 5D from the inlet. It means that the mesh with 36,000 elements give sufficient grid resolution for the solution, and it is chosen for further analysis. The result also agrees well with the theory equation as shown in Equation (2-13).

43

In order to ensure that a fully developed laminar flow is achieved, velocity profiles with mesh element equals to 36,000 at different locations (i.e. L = 0D, 2D, 5D, 6D, 8D, and 10D) are examined (see Figure 5.11). It is clearly seen that the velocity profiles at different streamwise locations are similar to each other. This shows that a fully similar developed laminar pipe flow has been achieved in the simulation.
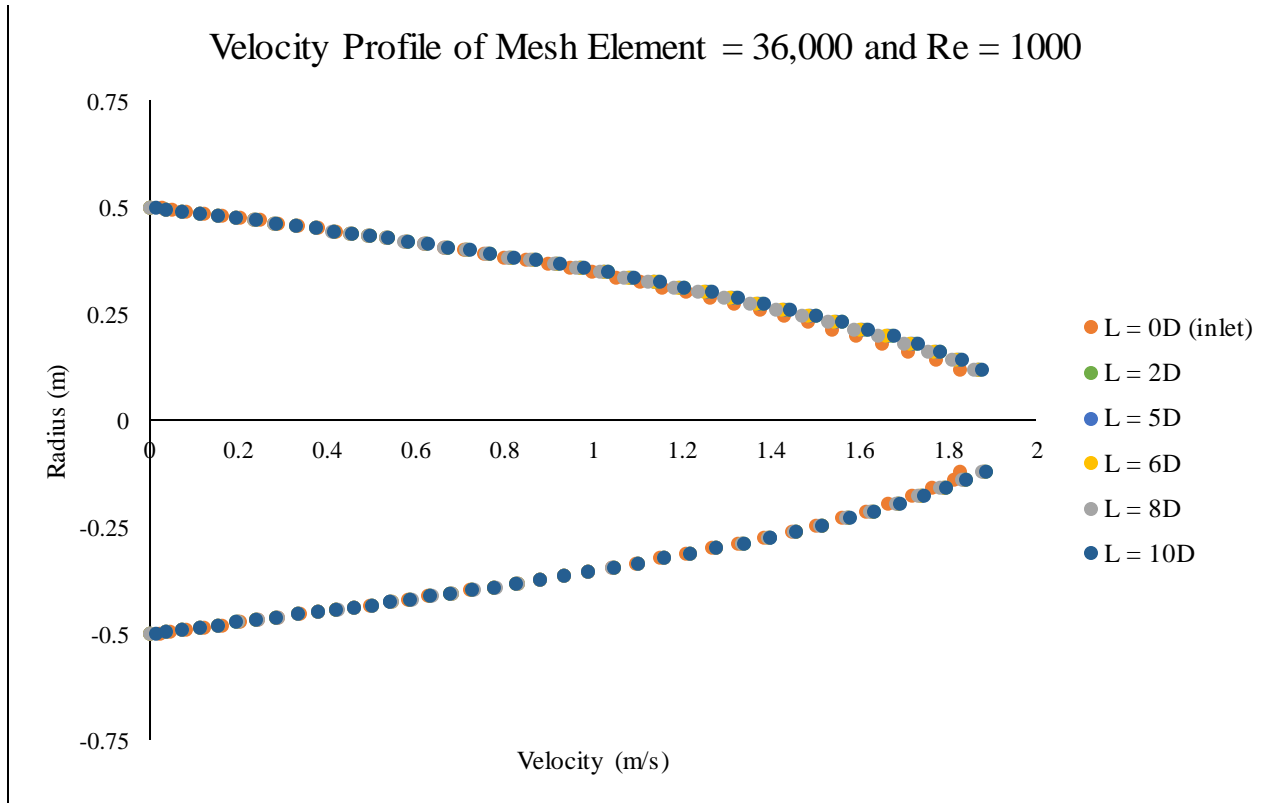


**Figure 5.11.** The Velocity Profile of 3-Dimensional Geometry with 36,000 Mesh Elements

The next study is to analyze the different time step (ΔT). The aim of this study is to determine which time step provides numerical stability when demonstrating the pimpleFoam solver. The requirement of this numerical stability is shown by the Courant number of less than 1. With the same simulation time of 400, the results are shown in the Table 5.3 and Figure 5.12.

**Table 5.3.** The Time Step (ΔT) and The Courant Number from PimpleFoam Simulation of 36,000 Mesh Elements

| ΔT (s) | Courant Number |
|---|---|
| 0.01 | 0.025 |
| 0.05 | 0.126 |
| 0.1 | 0.25 |
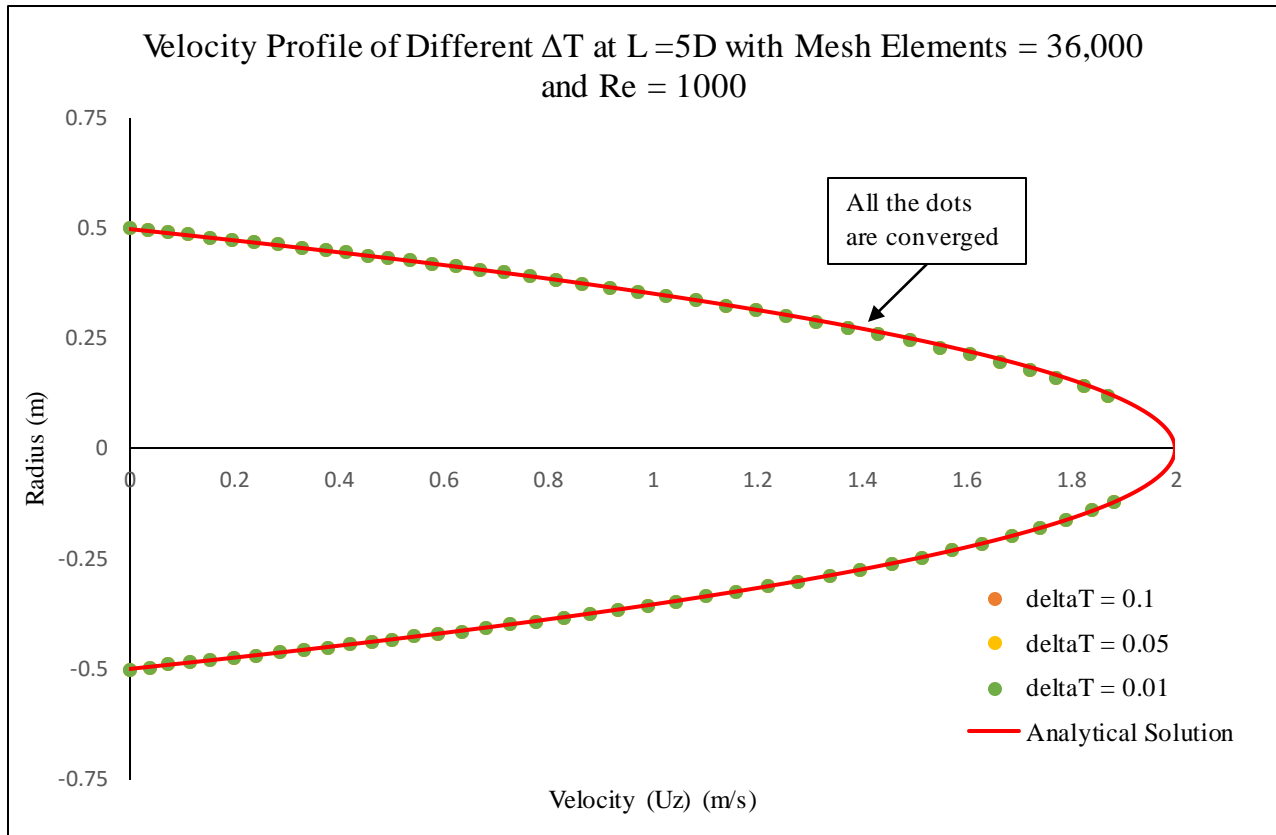
**Figure 5.12.** The Velocity Profile of 3-Dimensional geometry with Different Time Step (ΔT)

As shown in Figure 5.12, the velocity profiles (at location L = 5D from the inlet) with the ΔT = 0.01 s , ΔT = 0.05 s, and ΔT = 0.1 s are stable and converged with each other which are shown by the courant number less than 1 (See Table 5.3).
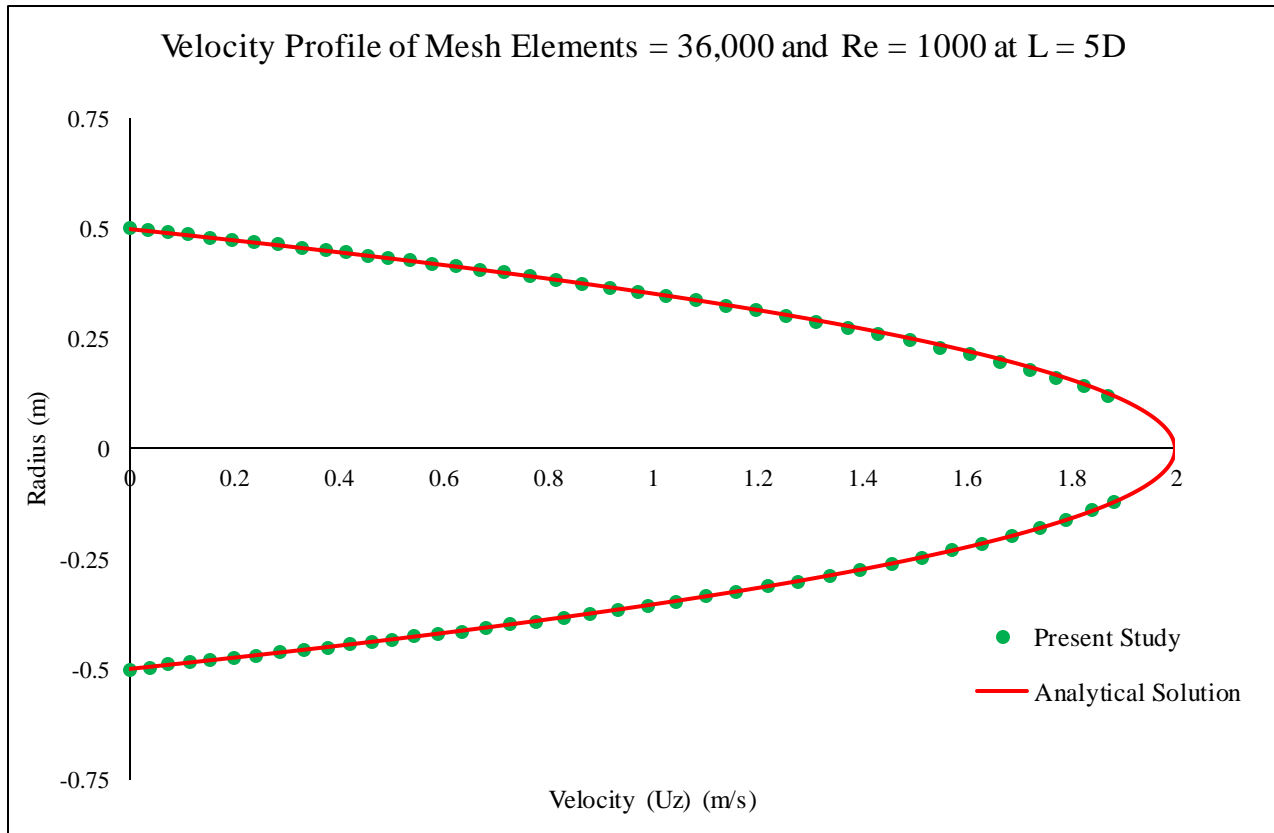
**Figure 5.13.** The Velocity Profile of the Present Study Vs the Analytical Solution at Location 5D from the Inlet

The results based on the analysis above, the velocity profile with the mesh element of 36,000 and time step ($\Delta T$) of 0.1 s can be selected for the further analysis. The $\Delta T = 0.1$ s is selected instead of $\Delta T = 0.01$ s and 0.05 s since the $\Delta T = 0.1$ s is faster to obtain convergence than the lower time step. The Figure 5.13 shows that the predicted velocity profile of the present study are in a good agreement with the analytical solution.

# Chapter 6.  Blind-tee and Elbow Pipe Case

## 6.1.    Introduction

According to Treloar (2010), blind-tee pipe is a tee installation with one of its branch connection blanked off. While, elbow pipe is one of the pipe fittings which has 90 degrees bent. Both blind-tee and elbow pipes are used to change the direction of the flow in piping. In this chapter, the physical fluid flow inside the blind-tee and elbow pipes are discussed.

## 6.2.    Methodology

Mainly, the procedure of analyzing the blind-tee and elbow pipe cases are the same as the straight pipe case. This case starts from creating the 3-D geometry of the pipes and setting up the mesh and the boundary condition of each studied pipes. After they are set properly, the next step is to perform the laminar flow analysis with PimpleFoam solver, then investigate whether the velocity profile at 10D from the inlet and 10D from the outlet region are merged in order to achieve the grid convergence study. After the velocity profile are merged, contour of the velocity and the pressure can be plotted. The methodology of the blind-tee and elbow pipe is shown in Figure 6.1.
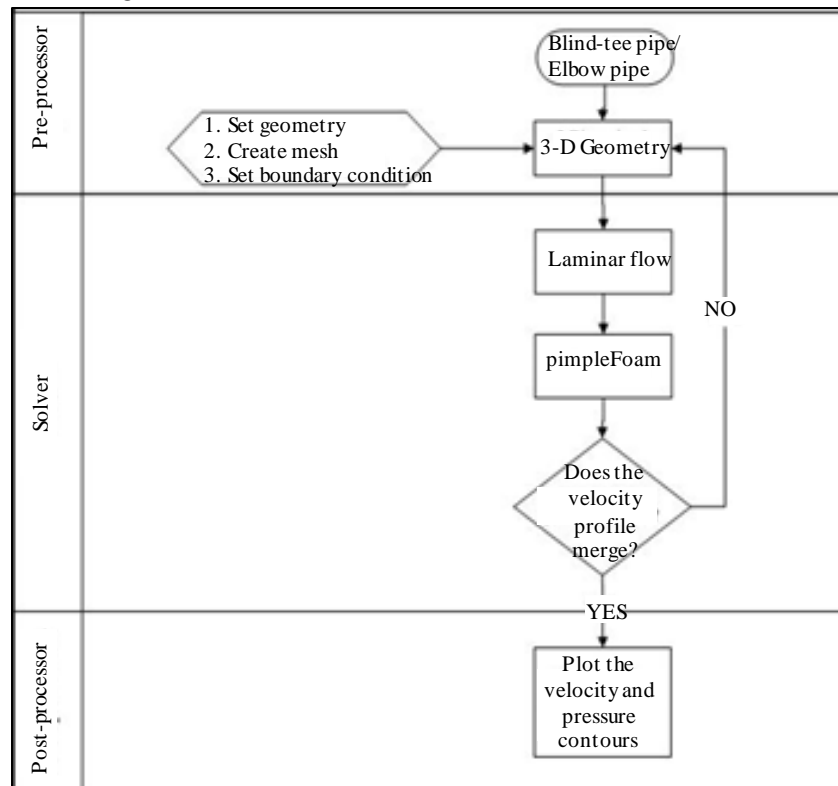


**Figure 6.1.** Methodology of Blind-tee and Elbow Pipe Case

## 6.3. Mesh set-up

The geometries of the blind-tee and elbow pipes are generated by utilizing Autodesk Inventor software. Furthermore, the mesh set up is done by using SALOME software. Considering the geometry of these pipes are more complex than the straight pipe case, the unstructured mesh is used for simulations. The mesh set up for the blind-tee and elbow pipe can be seen in Figure 6.2.



b)   Blind-tee                                    a)   Elbow Pipe
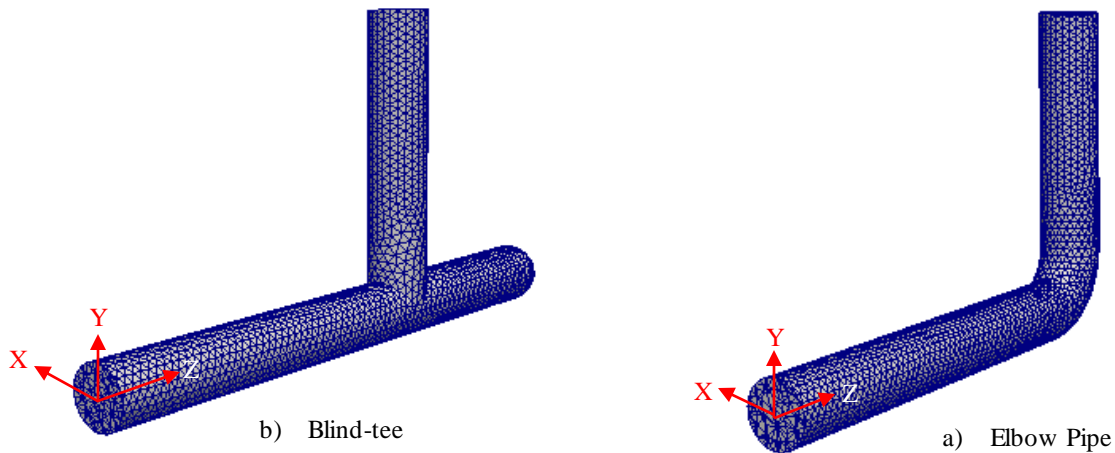
**Figure 6.2.** The Mesh Set-up for Blind-tee and Elbow Pipe Case

## 6.4. Sensitivity study

The laminar flow simulations for the blind-tee and elbow pipes case are carried out at Reynolds number = 1000. For the inlet velocity, the fully developed velocity profile which is obtained from the straight pipe case is used. The fluid flow inside these pipes experience velocity reduction during and inside the joint region. Therefore, the maximum velocity of the developed velocity profile in the blind-tee and elbow pipes case are lower than in the straight pipe case. The reduction of the velocity flow is due to the change of the pipe configuration. In order to perform the convergence in this case, the velocity profile of the straight pipe sections in z and y direction are compared. For the elbow pipe and blind-tee with the tee length (L tee) of 1D, 2D, and 3D, the velocity profiles are same at z = 15D and y = 15D (the location can be seen at Figure 6.3). Meanwhile, the blind-tee with L tee of 4D and 5D, the velocity profiles are same at z = 10D and y = 10D. The different location of the converged velocity is because of the length of the tee. Further analysis is to study whether the higher mesh elements will give impact to the velocity profile in order to achieve the grid convergence study.
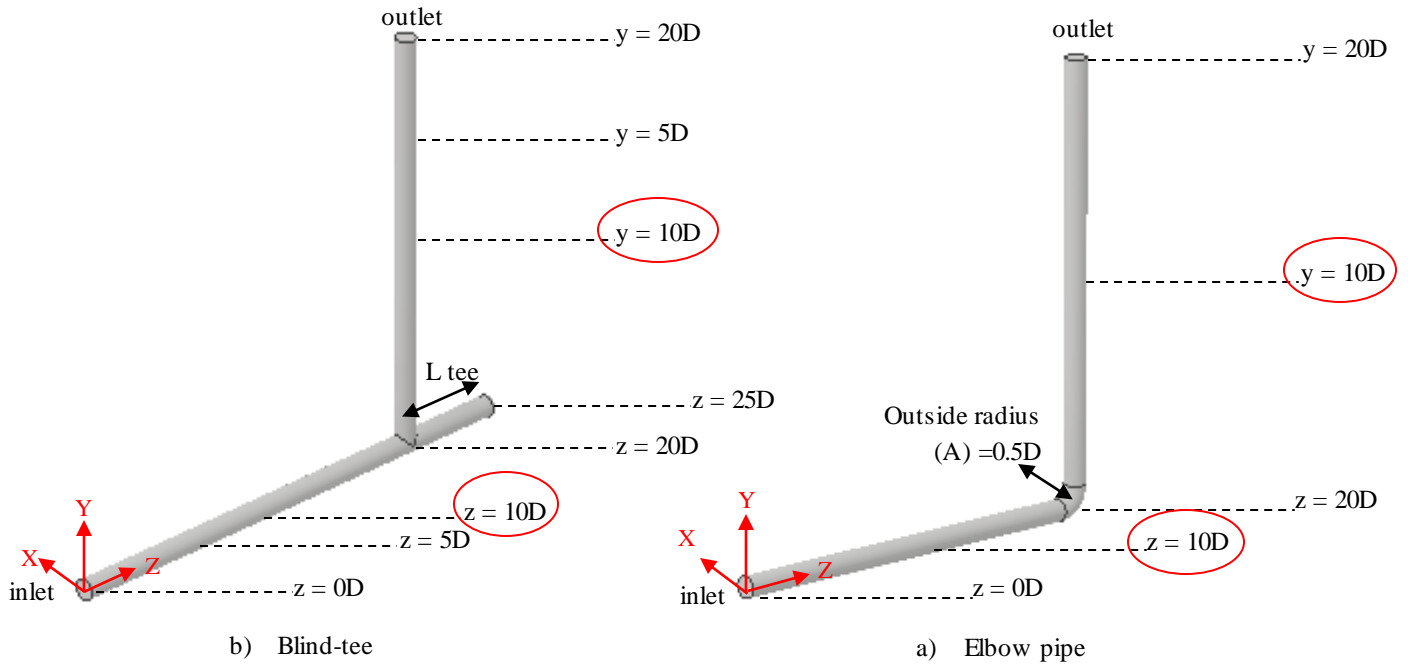
**Figure 6.3.** Location where the Velocity Profile from 2 Different Locations at z and y are Compared (Red Circle)

The list of the different mesh elements which are studied in this case is shown in Table 6.1. As the result, it can be seen in one of the blind-tee pipe cases (Blind-tee with L tee = 4D) in Figure 6.4. The velocity profiles for mesh = 30,564 and mesh = 67,445 are almost the same. It shows that a good grid convergence study has been performed for the simulations. The mesh with 30,564 elements is considered to have sufficient grid resolution. The result of the grid convergence study for other blind-tee pipe and elbow pipe cases are presented in Appendix A. The corresponding simulation results are chosen for further analysis and the comparison almost coincides with each other.

**Table 6.1.** Different Mesh Element Studies of Blind-tee and Elbow Pipe Case

| Blind-tee length | Mesh element (I) | Mesh element (II) |
| --- | --- | --- |
| 1 | 36,918 | 73,472 |
| 2 | 34,493 | 63,924 |
| 3 | 32,003 | 62,383 |
| 4 | 30,564 | 67,445 |
| 5 | 32,352 | 64,968 |
| 0 (elbow pipe) | 34,358 | 65,858 |
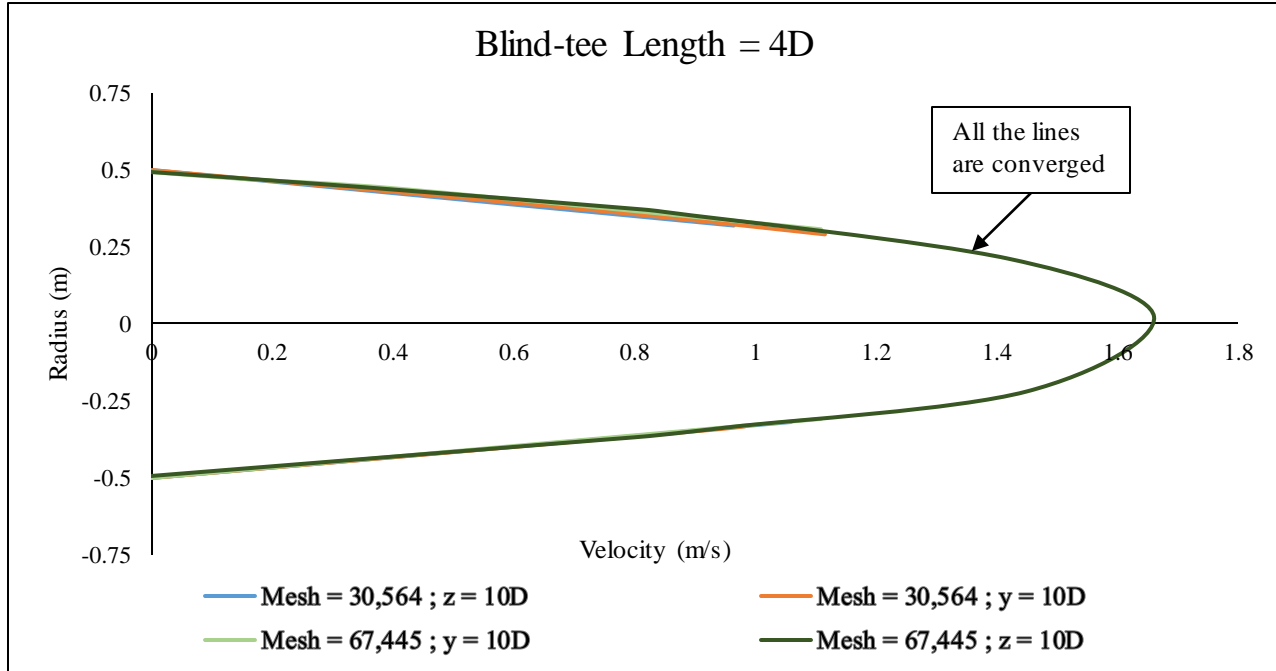
**Figure 6.4.** Convergence Graphs of the Velocity Profile of Blind-tee with Tee Length = 4D

## 6.5. Result and discussion

This section presents the results of the physical flow inside the blind-tee and elbow pipes. The laminar flow simulations for the blind-tee and elbow pipes case are carried out at Reynolds number = 1000. The velocity streamline of blind-tee with L tee = 1D to 5D are shown in Figure 6.5 (a) to (e) and elbow pipe is shown in Figure 6.5 (f). The different colors of the streamlines inside the pipe represent different velocity values in z direction (Uz). The velocity (Uz) contour ranges from -0.8 m/s to 2m/s.

By plotting the streamlines of the fluid flow inside the studied pipes, the behavior of how the fluid is flowing can be seen clearly. The streamlines of the flow inside these blind-tee and elbow pipes depict differently. It can be seen that the streamlines coming from the inlet, show straight lines. When they reach the blind-tee shape, some fluid flows towards the outlet and some fluid flows towards the blind-tee.

Since one of the branches of the blind-tee is blanked-off, the fluid is trapped in this part. As the result, when the fluid flow hits the blanked-off side, it flows back and creates flow circulation. However, the fluid which

flows inside the elbow pipe, does not create any flow circulation. The elbow pipe which is studied in this case has R/A = 1 and Dean number (De) = 1000.

The flow circulation inside the blind-tee, shows different sizes according to the length of the tee. For the blind-tee with L tee = 1D, the diameter of the circulation size is 1D. The blind-tee with L tee = 2D, the diameter of the circulation size is 2D. The blind-tee with L tee = 3D, the diameter of the first flow circulation size is 2D. Moreover, the second flow circulation with the size of 0.5D is formed even though it appears to have vague shape. For the blind-tee with L tee = 4D, it can be seen clearly that the two flow circulations have occurred. The first flow circulation size inside this particular blind-tee, has diameter size equals to 2D. Moreover, the second flow circulation, has diameter size of 1.5D. It can be seen clearly also that the flow circulation inside the blind-tee with L tee = 5D, creates three circulations, with the diameter of 2D, 1.5D and the third circulation starts to develop.

It can be concluded from the streamlines plot in Figure 6.5, the flow is trapped inside the blind-tee and it flows freely towards the outlet in the elbow pipe. The flow which is trapped inside the blind-tee with L tee equals to 1D and 2D will form one flow circulation, while in the L tee of 3D to 5D, the flow will form more than two flow circulations. In the blind-tee with tee length of 3D and 4D, two circulations are formed, since the maximum capability of the first flow to create circulation inside this pipe is only limited on the size of 2D. Therefore, other flow circulations are created. Furthermore, at locations near the blanked-off wall which is 0.5D from the blanked-off wall, there is no flow circulation occurring because the velocity at this location is very low and almost zero. Hence, it can be said that stagnant velocity happens at the location 0.5D from the blanked-off wall towards the incoming flow.

a) Blind-tee length = 1D    b) Blind-tee length = 2D

c) Blind-tee length = 3D    d) Blind-tee length = 4D

e) Blind-tee length = 5D    f) Elbow Pipe
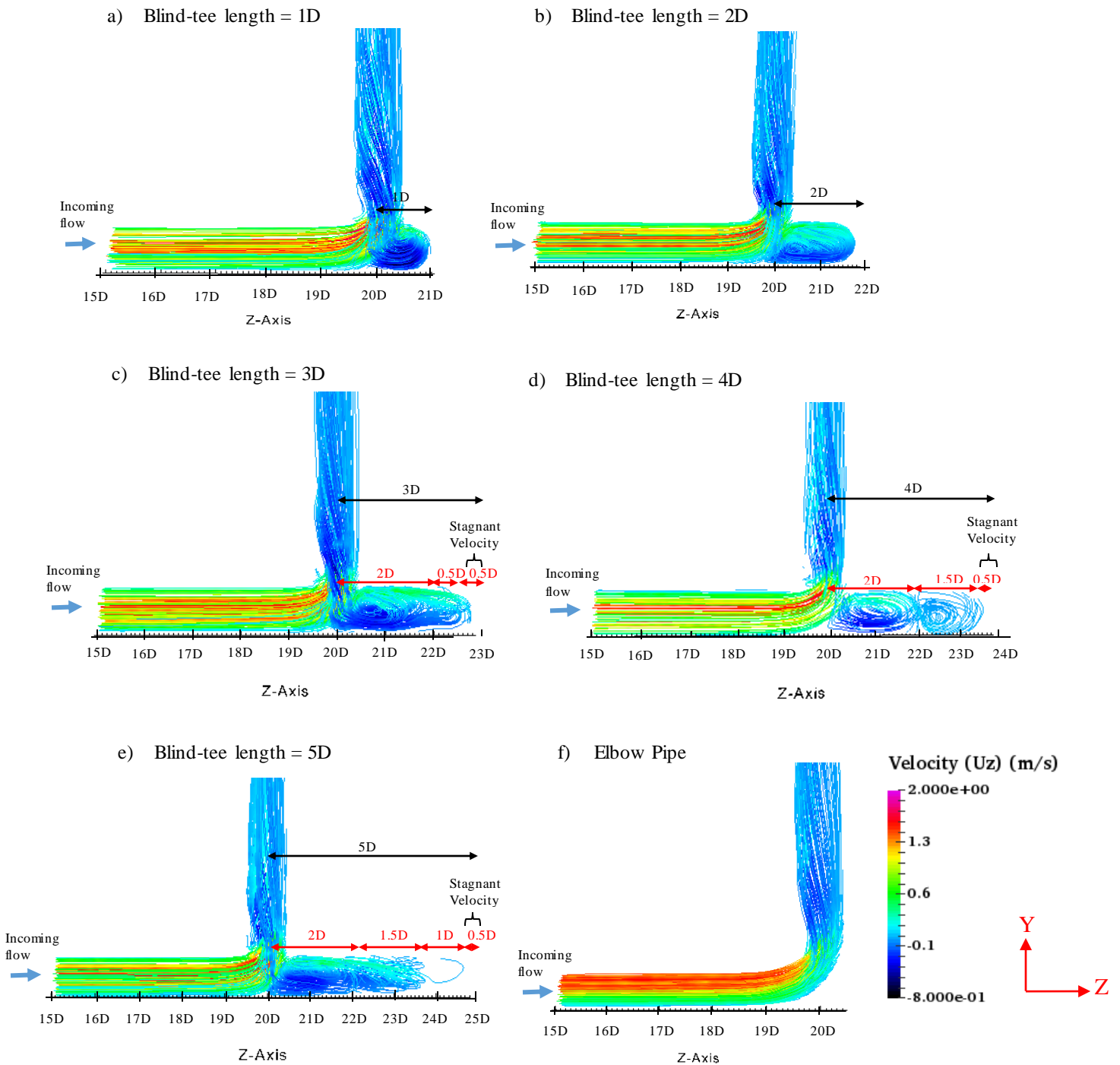
**Figure 6.5.** Velocity Streamline of Blind-tee and Elbow Pipe Colored by Uz Contour

In order to understand at which location the flow circulation starts to develop, the velocity streamline of the blind-tee pipes with L tee less than 1D are presented in Figure 6.6. In this Figure, the elbow pipe which acts as the blind-tee with L tee = 0D is also shown. For the blind-tee with L tee = 0D, the main flow is flowing directly to the outlet without any separation. The flow behavior at the blind-tee with L tee = 0.25D, is similar to the blind-tee with L tee = 0D which the separation effect does not happen in the blind-tee section. The

52

blind-tee with L tee = 0.5D the separation effect and the flow circulation start to develop. Furthermore, in the blind-tee with L tee = 0.75D, the flow circulation is developed completely. Thus, it can be concluded that the flow circulation inside the blind-tee pipe starts to develop in L tee = 0.5D and completely develop in L tee more than 0.75D.

a)  Elbow Pipe/ Blind-tee with L tee = 0D

b)  Blind-tee length with L tee = 0.25D

c)  Blind-tee with L tee = 0.5D

d)  Blind-tee with L tee = 0.75D
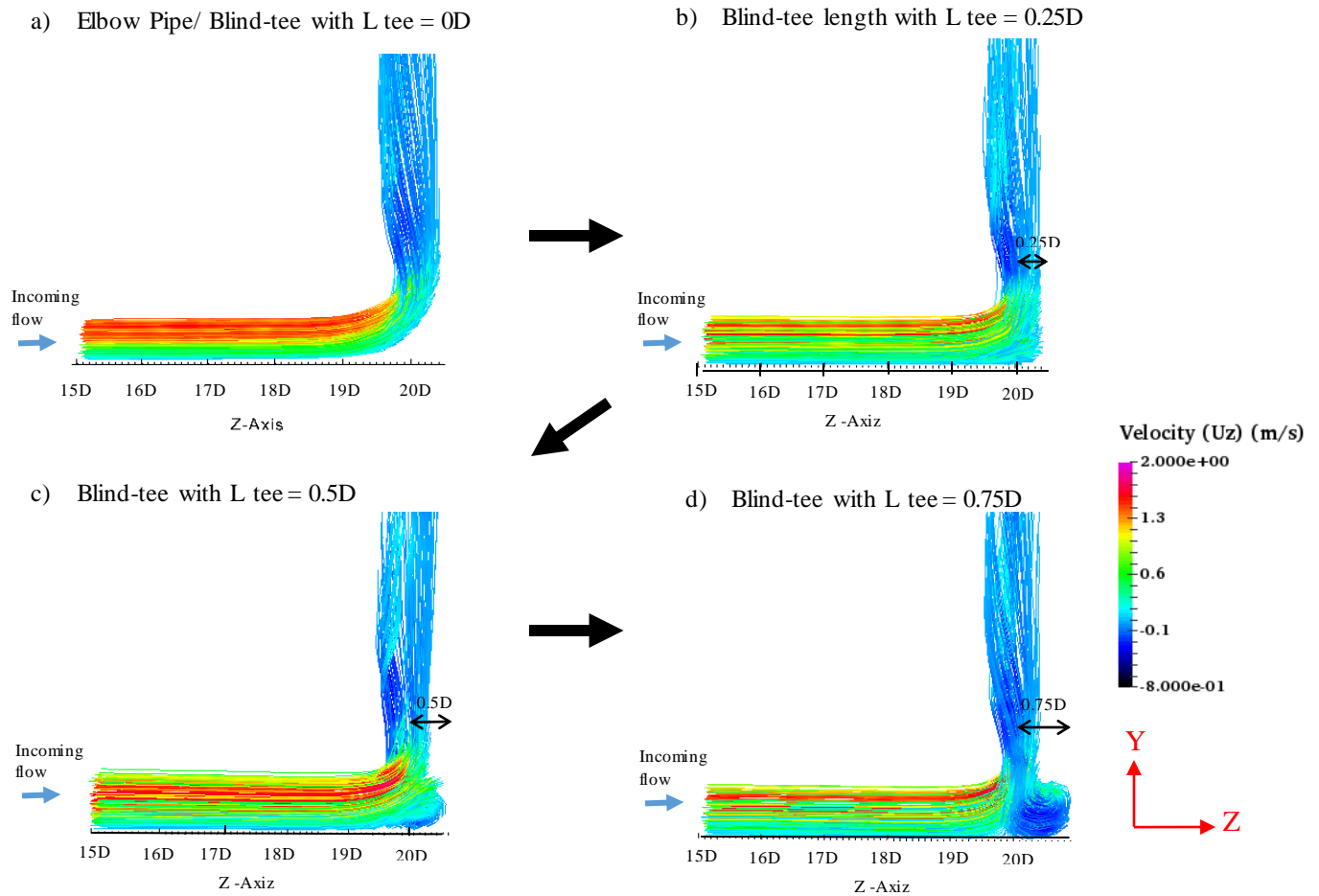


**Figure 6.6.** The Development of Velocity Streamline in Blind-tee Pipes colored by Uz Contour

Figure 6.7 depicts the flow circulations pattern which happen beyond the blind-tee with L tee = 5D. The aim of this analysis is to understand at which location the flow circulation stops to develop. In the blind-tee length equals to 6D and 8D there are two flow circulations occurring in the blind-tee section. The first flow circulation has diameter size of 2D and the second flow circulation has diameter size of 1.5D. While, for the blind-tee with L tee = 10D, there are three flow circulations which the diameter size of first flow circulation is 2D, the second flow circulation is 1.5D and the third flow circulation is 1D. However, the third flow circulation is weak and not so obvious. It can be seen that at the location more than 24D until the blanked-off wall of the pipe, there are no flow circulations or even streamlines in this location. This is because the velocity

of the flow in this region is very low and almost zero, thus it can be said that in this location the velocity is stagnant. In Figure 6.7, the flow circulation pattern of sizes can also be observed which are for the first flow circulation the diameter size is 2D and for the second flow circulation the diameter size is 1.5D. By comparing the L tee = 8D and 10D, the third flow circulation at L tee = 10D cannot be determined in this study since it requires longer blind-tee pipe to be studied.

a)  Blind-tee with L tee = 6D (Uz Streamline)    Blind-tee with L tee = 6D (Uz Contour)

b)  Blind-tee with L tee = 8D (Uz Streamline)    Blind-tee with L tee = 8D (Uz Contour)

c)  Blind-tee with L tee = 10D (Uz Streamline)   Blind-tee with L tee = 10D (Uz Contour)

**Figure 6.7.** The Uz Streamline and Pressure Contour of Blind-tee Pipes with L Tee = 6D, 8D, and 10D

The next analysis is to study the velocity and pressure difference inside the blind-tee and elbow pipes case. Figure 6.8 and Figure 6.9 exhibits the velocity in z direction (Uz) and pressure contour of the flow inside the studied pipes from z = 5D (for elbow pipe and blind-tee with L tee = 1D, 2D, and 3D) and z = 10D (for blind-tee with L tee = 4D and 5D). The velocity (Uz) contour ranges from -0.8 m/s to 1.3 m/s and the pressure contour ranges from 0.8 Pa to 3 Pa.

Figure 6.8 and Figure 6.9 show clearly the velocity and pressure contour of the flow inside each blind-tee and elbow pipes. In general, the maximum velocity values of the flow from the inlet which has straight pipe s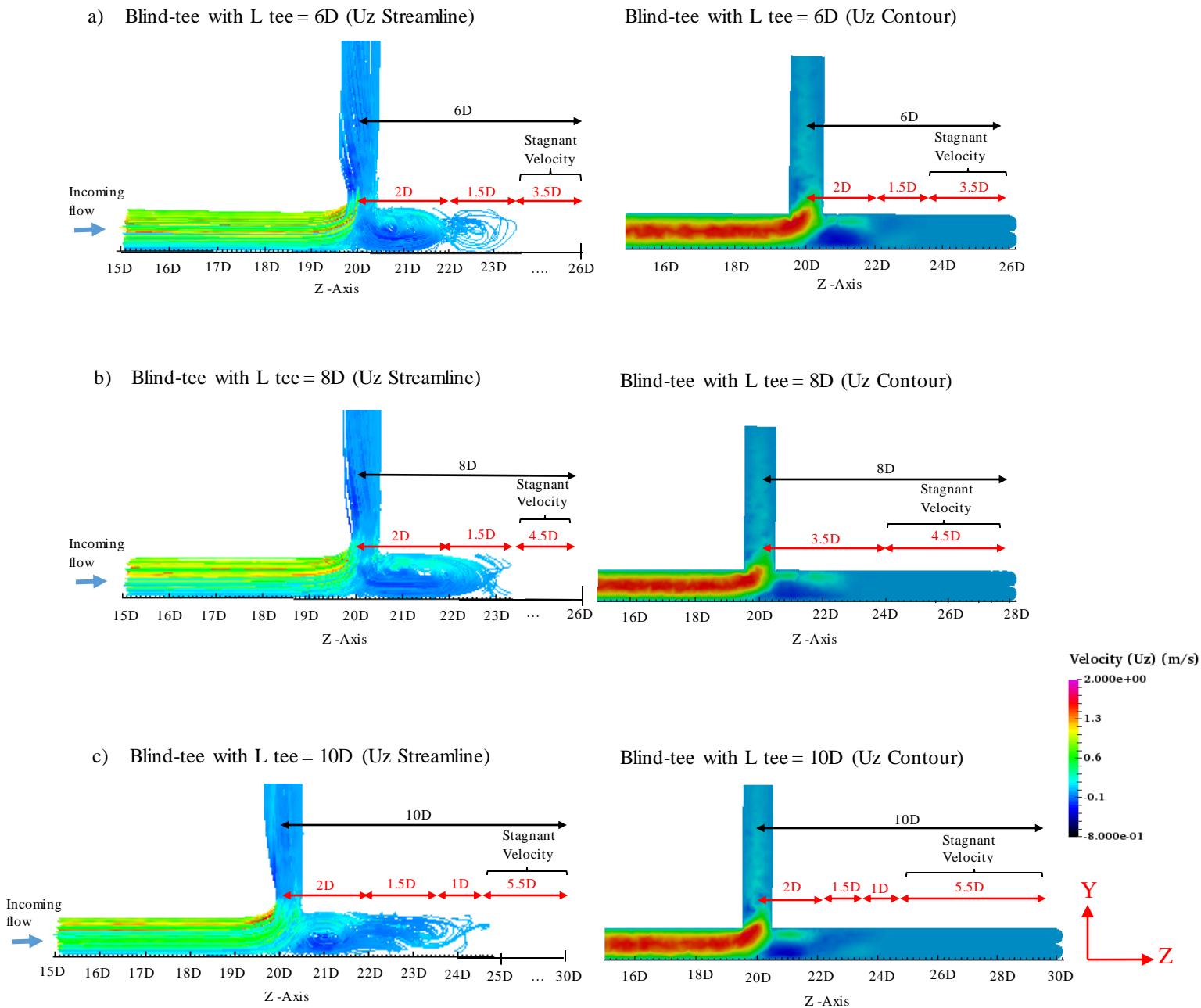haped, is Uz ≈ 1.65 m/s, and it is gradually reduced during the pipe fittings or pipe joints (blind-tee and elbow). It can be seen that the velocity at the flow inside the blind-tee with the L tee = 1D at location 20.5D, mainly depicts two different color, green and dark blue. They represent the maximum velocity inside this blind-tee is 0.76 m/s and (-)0.76 m/s (see Figure 6.10). These two different directions describe the flow circulation which occurs inside the blind-tee. For the blind-tee with L tee = 2D and 3D, the two velocity value differences are also shown even though the area of the green color at the upper part of the pipe is smaller than the blue color at the lower part of the pipe. These different velocity flow distributions show that at the lower part of the pipe, the flow velocity is higher than the upper part. This because, as consequence of the dividing flow from the main flow that happens in the pipe's intersection that can be seen clearly in Figure 6.8. This flow comes from the inlet then hits the corner of the blind-tee and separates to the outlet and inside the blind-tee. The fluid which is coming to the blind-tee, flows near to the wall. Therefore, the velocity at the upper part of this pipe becomes smaller than the lower part. The maximum velocity of blind-tee with L tee = 2D at the upper part is 0.39 m/s and at the lower part is -0.59 m/s. The maximum velocity of blind-tee with L tee = 3D at the upper part is 0.44 m/s and at the lower part is -0.65 m/s.

For the blind-tee with the L tee = 4D and 5D (see Figure 6.9), they have the same velocity distribution as the blind-tee with L tee = 2D and 3D at the location from 20.5D to 22D. Whereas, for blind-tee with L tee = 4D between the location 22D and 23.5D, the velocity contour area at the upper part of the pipe is wider than at the lower part. It means that the velocity at the upper part is higher than at the lower part of the pipe. The maximum velocity (Uz) at the upper part is -0.03 m/s and at the lower part is 0.019 m/s. Furthermore, for the blind-tee with L tee = 5D, the maximum velocity (Uz) at the upper part is 0.15 m/s and at the lower part is -0.27 m/s. However, at location between 23.5D and 24.5 D, the maximum velocity (Uz) at the upper part is 0.013 m/s and at the lower part is -0.02 m/s. From the result above at the location near the blanked-off tee of L tee equals to 4D and 5D, the maximum velocity is near to zero. It means that the fluid in this location is stagnant. As consequence, fluid or other substance will be deposited.

The pressure contours which are exhibited in Figure 6.8 and Figure 6.9, show that the pressure around the pipe junctions are smaller than the pressure at the inlet. These are depicted by different color contour that is

shown in the Figure 6.8. As it is shown in the blind-tee with L tee = 1D, the average pressure at the center of the pipe at z = 20.5D is 1.95 Pa. While, the average pressure at z = 15D, is 3 Pa. Thus, the pressure drop which occurs at z = 20.5D equals to 1.05 Pa. Moreover, for other blind-tee and elbow pipes, the pressure difference also occurs at the same location (z = 20.5D). For blind-tee with L tee = 2D, the pressure drop = 0.51 Pa; blind-tee with L tee = 3D, the pressure drop = 0.44 Pa; blind-tee with L tee = 4D, the pressure drop = 0.29 Pa; blind-tee with L tee = 5D, the pressure drop = 0.14 Pa; and for elbow pipe, the pressure drop at z = 0.5D equals to 0.78 Pa. However, the pressure which occurs at the corner of the blind-tee pipe is higher than its surroundings which is shown as red color (Uz ≈ 2.7 Pa). This happens since there is gap in the corner where the velocity occurs in this region is very low. Furthermore, at the location near the blanked-off part, the pressure values are higher than the pressure value around the pipe junctions. This is because the magnitude velocity inside this part is very low.
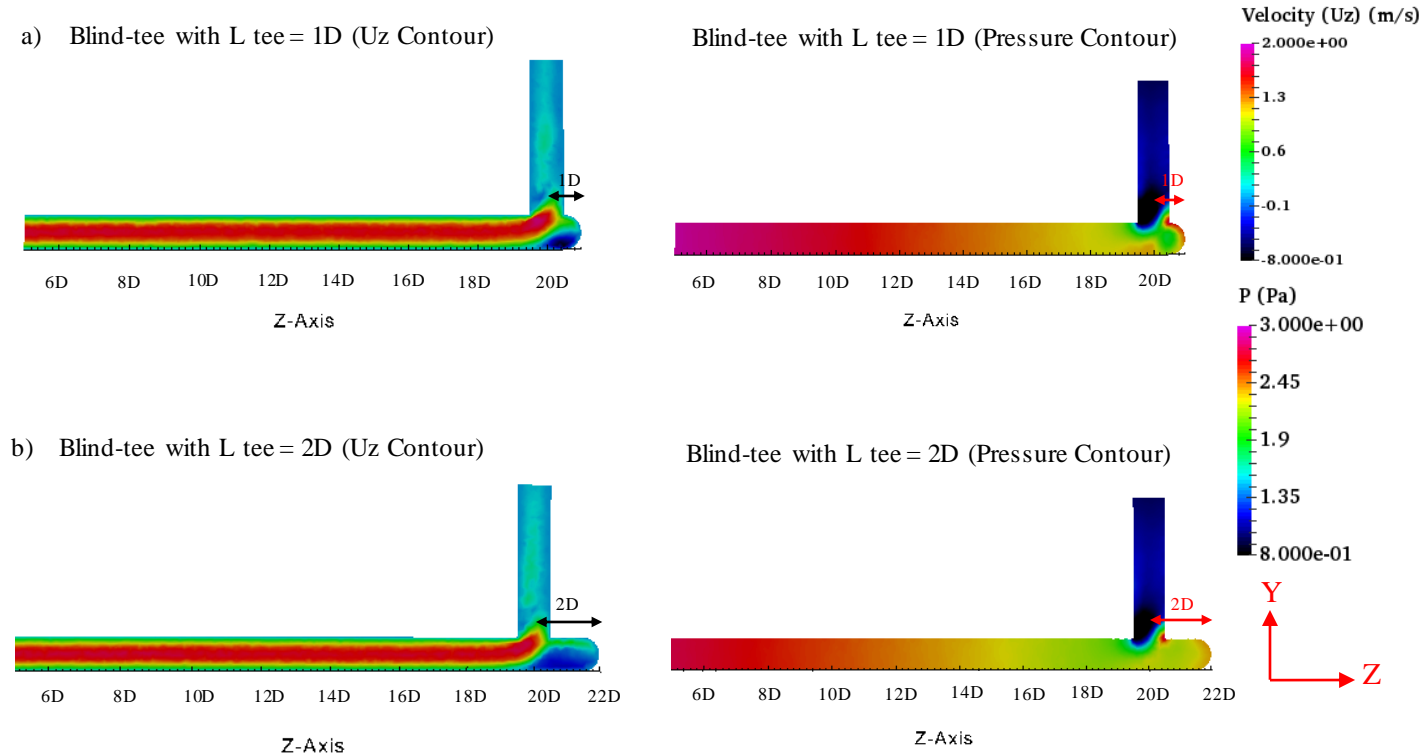


**Figure 6.8.** Uz and Pressure Contour of Blind-tee Pipes

c)  Blind-tee with L tee = 3D (Uz Contour)          Blind-tee with L tee = 3D (Pressure Contour)

d)  Blind-tee with L tee = 4D (Uz Contour)          Blind-tee with L tee = 4D (Pressure Contour)

e)  Blind-tee length = 5D (Uz Contour)              Blind-tee length = 5D (Pressure Contour)

f)  Elbow Pipe (Uz Contour)                         Elbow Pipe (Pressure Contour)
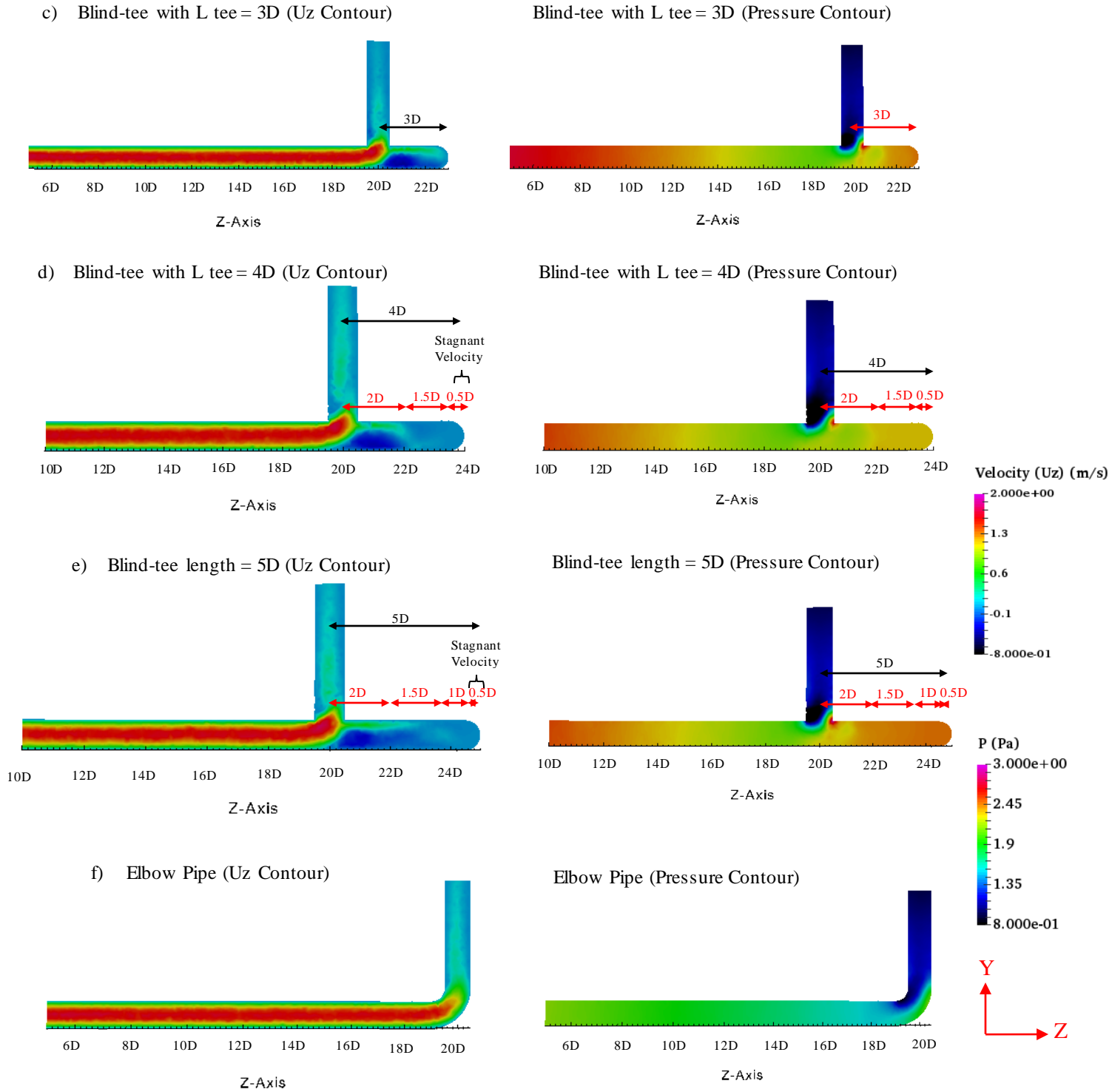


**Figure 6.9.** Velocity and Pressure Contour of Blind-tee Pipes and Elbow Pipe

57

Figure 6.10 depicts the comparison of velocity distribution between two locations at 5D from the inlet and at 20.5D of blind-tee with L tee = 1D. It can be seen that at the location of 20.5D, there are two different directions of flow which at the upper part of the pipe the fluid is flowing in the same direction with z axis. The lower part of the pipe, the flow is flowing in the opposite direction with z axis. Hence the sign of the velocity is negative. This shows that at the location of 20.5D there is flow circulation. If these two velocities at the locations inside the blind-tee are compared with the location of 5D from the inlet, it is found that the velocities at z = 5D have only one direction. This is because, there is no flow circulation that occurs before the blind-tee.

a)   z = 20.5 D                                          b)   z = 5D
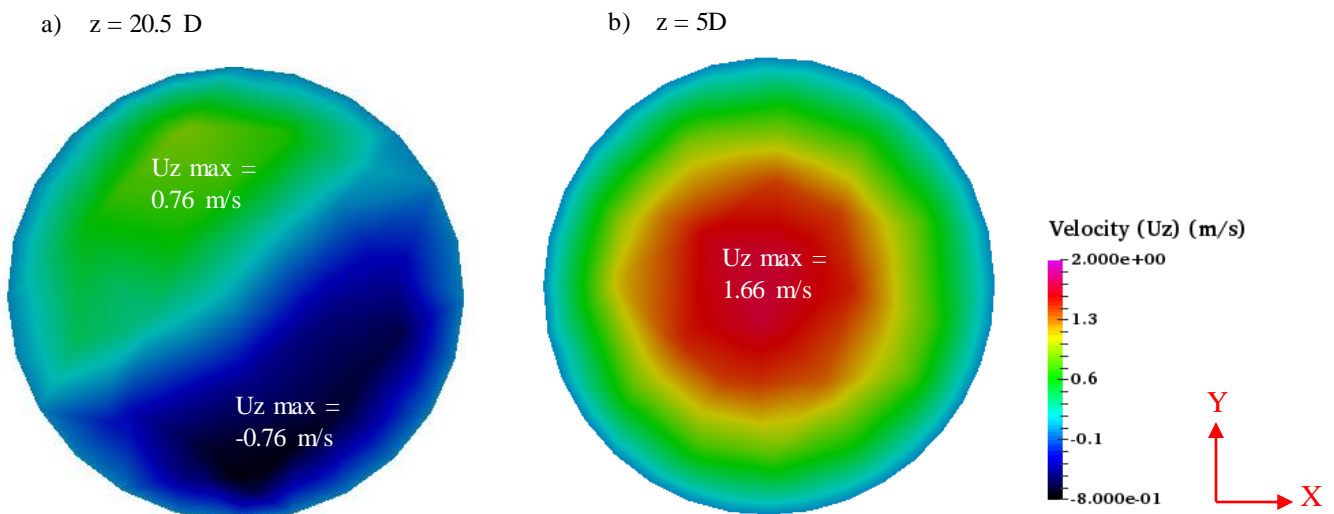


**Figure 6.10.** The Comparisson Velocity between Location Z = 20.5D and Z = 5D of Blind-tee with L tee =1D

Figure 6.11 exhibits the comparison of the velocity and pressure contours of cross section between two locations inside the blind-tee with L tee = 4D. The blind-tee with L tee = 4D is chosen since the two circulations of flow in this blind-tee start to develop completely. It can be seen that the velocity values at z = 21D from the inlet and z = 23D from the inlet show two different directions at the upper and lower part of the pipe. At z = 21D, the maximum velocity at the upper part is 0.4 m/s and at the lower part, the maximum velocity is -0.58 m/s. At z = 23D, the maximum velocity at the upper part of the pipe is -0.03 m/s and at the lower part, the maximum velocity is around 0.019 m/s. This shows that at z = 23D, the flow experiences reversed flow circulation from the flow at z = 21D. The average pressure (P) at z = 21D equals to 2.175 Pa, and at z = 23D, the average pressure equals to 2.3 Pa. The pressure at z = 23D is higher at z = 21D is because the maximum velocities at z = 23D are lower than at z = 21D which are 0.019 m/s and -0.03 m/s.

a)  z = 21D
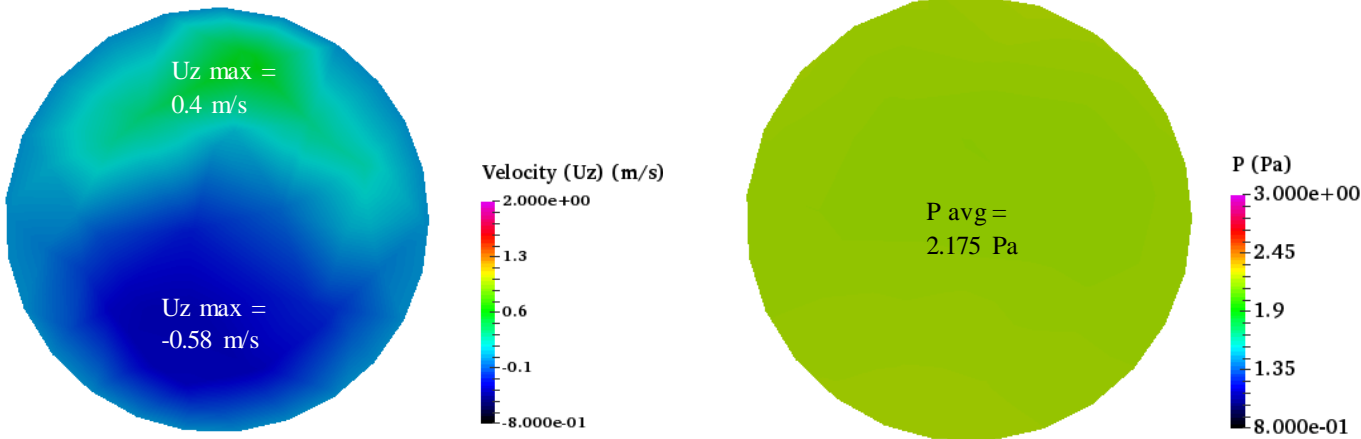


b)  z = 23D
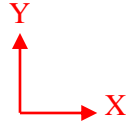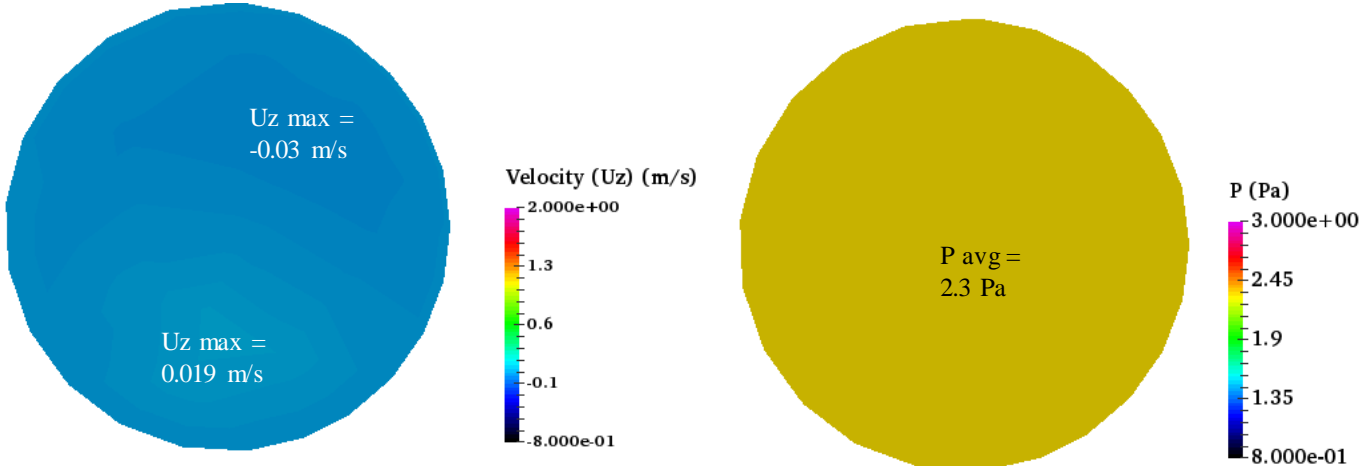


**Figure 6.11.** Velocity and Pressure Contour of Blind-tee Pipe with L Tee = 4D

# Chapter 7. Conclusion and Recommendation for Future Study

## 7.1. Conclusion

In this thesis, three-dimensional numerical simulation of fluid flow in the straight pipe, blind-tee, and elbow pipes have been presented. The analysis of the physical flow obtained using the OpenFOAM software have been made. The conclusion of the analysis is presented as follow:

1. Mesh set-up for the pipe geometries should be conducted properly in order to achieve correct velocity profile.
2. In order to reduce the simulation time effectively, the fully developed laminar pipe flow from the analytical solution of classical formula is taken as an input at the inlet.
3. PimpleFoam solver in OpenFoam is suitable to be used for laminar flow simulation.
4. The velocity profile in the straight pipe agrees well with the analytical solution of the classical formula.
5. For analyzing laminar flow in the complex geometry pipe, the unstructured mesh can be used.
6. The streamline, velocity contour, and pressure contour are presented for the blind-tee and elbow pipe case.
7. Flow circulations happen inside the blind-tee.
8. The flow is trapped inside the blind-tee and it flows freely in the elbow pipe. The flow which is trapped inside the blind-tee with L tee equals to 1D until 3D will form one circulation, while in L tee of 4D and 5D, the flow will form more than one circulations.
9. The flow circulation size inside the blind-tee has its pattern which the first circulation has diameter size of 2D and the second circulation has diameter size of 1.5D.
10. The blind-tee with tee length equals to more than 4D, has potential to create fluid deposit since the velocity of the flow is very low (almost zero).
11. The flow circulation starts to develop completely in the blind-tee with L tee equals to 0.75D.

## 7.2. Recommendation for future study

This section consists of recommend scope of works that should be done in future works. The following lists are some of the scope of works that should be done for further studies:

1. Since this thesis is only limited to laminar flow analysis, there can be more work done with the CFD simulation for turbulent flow analysis.
2. Experimental study of pressure drop in the blind-tee pipes shall be conducted with more detailed analysis.
3. The analysis of the flow inside pipe with other different pipe fittings such as Y-fitting and 45-degree elbow can be done in the future study.
4. Other analysis of flow inside pipe such as the analysis of internal flow of pipe which has various shapes of obstacles are suggested.
5. The corrosion and corrosive as the impact of deposit fluid inside the blind-tee can be simulated in the future work.

# References

Bakker, A., 2006. *Applied Computational Fluid Dynamics: Meshing.* [Online]
Available at: http://www.bakker.org/dartmouth06/engs150/07-mesh.pdf
[Accessed 24 April 2016].

Bengston, H., 2010. *Bright Hub Engineering.* [Online]
Available at: http://www.brighthubengineering.com/hydraulics-civil-engineering/55543-pipe-flow-calculations-1-the-entrance-length-for-fully-developed-flow/
[Accessed 10 April 2016].

Cade, M., Lima, W., Farias Neto, S. & Lima, A., 2010. Natural Gas Laminar Flow in Elliptic Cylindrical Pipes: A Numerical Study. *Brazilian Journal of Petroleum and Gas,* Volume 4, pp. 19-33.

Campbell, W. D. & Slattery, J. C., n.d. Flow in the Entrance of a Tube. *ASME Paper No. 62-Hyd-6.*

Cengel, Y. & Cimbala, J., 2014. *Fluid Mechanics.* 3rd ed. Singapore: Mc Graw Hill Education.

CFD-Online, 2007. *CFD-Online: Mesh Classification.* [Online]
Available at: http://www.cfd-online.com/Wiki/Mesh_classification
[Accessed 24 April 2016].

CFD-Online, 2012. *CFD-online.* [Online]
Available at: http://www.cfd-online.com/Wiki/Direct_numerical_simulation_(DNS)
[Accessed 13 March 2016].

CFD-Online, 2012. *CFD-Online, Mesh.* [Online]
Available at: http://www.cfd-online.com/Wiki/Mesh
[Accessed 24 April 2016].

CFDsupport, 2016. *CFDsupport.* [Online]
Available at: http://www.cfdsupport.com/why-openfoam.html
[Accessed 18 March 2016].

Ferziger, J. & Peric, M., 1999. *Computational Methods for Fluid Dynamics.* 2nd ed. s.l.:Springer.

Foias, C., Manley, O., Rosa, R. & R., T., 2001. *Navier-Stokes Equation and Turbulence.* Cambridge: Cambridge University Press.

Friedmann, M., Gillis, J. & Liron, N., 1968. Laminar Flow in a Pipe at Low and Moderate Reynolds Numbers. *Applied Scientific Research,* 19(1), pp. 426-438.

Gary, J. & Handwerk, G., 1984. *Petroleum Refining Technology and Economics.* 2nd ed. s.l.:Marcel Dekker, Inc..

Greenshields, C. J., 2011. *OpenFOAM The Open Source CFD Toolbox: User Guide,* s.l.: CFD, Direct Ltd..

Hornbeck, R., 1964. Laminar Flow in The Entrance Region of a Pipe. *Applied Scientific Research,* pp. 224-232.

Livelli, G., 2010. *Flow Control: Flowmeter Piping Requirements.* [Online]
Available at: http://www.flowcontrolnetwork.com/flowmeter-piping-requirements/
[Accessed 3 May 2016].

Lysenko, D., I.S., E. & E., R. K., n.d. *Turbulent Bluff Body Flows Modeling Using OpenFOAM Technology.* [Online]
Available at:
https://www.google.no/url?sa=t&rct=j&q=&esrc=s&source=web&cd=1&ved=0ahUKEwie3KGo4ZXNAh WDQZoKHVztDiQQFggfMAA&url=http%3A%2F%2Fwww.decgroup.org%2Fpapers%2Fmekit11_lysen ko_paper.pdf&usg=AFQjCNEkT-q2HjXx051E9PlfcLllSF4r3g&sig2=ubRURnWtfxmr0Ox7a1gDYQ&cad=rjt
[Accessed 25 April 2016].

Mehul, P., 2013. *H-Tech Outsourcing Services.* [Online]
Available at: http://www.hitechcfd.com/cfd-knowledgebase/seven-stages-of-a-typical-cfd-simulation.html
[Accessed 20 March 2016].

Olsen, T., 2014. An Oil Refinery Walk-Through. *AIChE Publication,* pp. 34-40.

OpenFOAM, 2009. the Open Source CFD Toolbox, Programmer's Guide. *OpenCFD Limited,* Volume Version 1.6.

OpenFOAM, 2011. *OpenFOAM : Standard Solvers.* [Online]
Available at: http://www.openfoam.org/features/standard-solvers.php
[Accessed 2 May 2016].

Patel, M., 2013. *CFD Modeling Services.* [Online]
Available at: https://cfdmodelingservices.wordpress.com/2013/06/12/4-advantages-and-disadvantages-of-cfd/
[Accessed 17 March 2016].

Pipestock, 2004. *Pipestock.com.* [Online]
Available at: https://www.pipestock.com/stainless-steel/150lb-316-stainless-steel-pipe-fittings/equal-tee
[Accessed 26 January 2016].

Prandtl, L. & Thetjens, O. G., 1957. *Applied Hydro- and Aeromechanics.* New York: Dover.

Prinsco, 2016. *Prinsco.* [Online]
Available at: http://www.prinsco.com/prinsco-markets/fittings-accessories/blind-tee-civil-commercial-construction/
[Accessed 2 February 2016].

Robertson, A. & Galdi, G., 2005. On Flow of a Navier-Stokes Fluid in Curved Pipes. Part I: Steady Flow. *Elsevier,* pp. 1116-1124.

Samsung-Engineering, 2013. *Samsung Engineering - Business Portofolio.* [Online]
Available at: http://www.samsungengineering.co.kr/business/unit/common/buView
[Accessed 1 May 2016].

Shearer, J., 2014. *Basic Blueprint Reading.* [Online]
Available at: http://www.slideshare.net/jcshearer/basic-blueprint-reading
[Accessed 25 May 2016].

Shirayama, S. & Kuwahara, K., 1987. Computational Study of Flow in a Curved Pipe with Circular Cross Section. *KSME Journal,* Volume 1, pp. 52-59.

Singh, V. P., 1996. *Kinematic Wave Modeling in Water Resources: Surface Water Hydrology*. Canada: John Wiley & Sons, Inc.

Spedding, P., Benard, E. & G.M., M., 2004. Fluid Flow through 90 Degree Bends. *Dev. Chem. Eng. Mineral Process,* pp. 107-128.

Temam, R., 1984. *Navier-Stokes Equations: Theory and Numerical Analysis*. Amsterdam: North-Holland.

Tennekes, H. & J.L., L., 1992. *A First Course in Turbulence*. Cambridge MA: The MIT Press.

Thaker, A. & J., B. B., 2011. Numerical Simulation of Flow in Lid-driven Cavity using OpenFOAM. *Insitiut of Technology, Nirma University, Ahmedabad.*

Treloar, R., 2010. *Gas Installation Technology*. 1st ed. New Delhi: Wiley-Blackwell.

Tu, J., Yeoh, G. & Liu, C., 2007. *Computational Fluid Dynamics: A Practical Approach*. 1st ed. Oxford: Elsevier Inc..

Vasava, P., 2007. *Fluid Flow in T-Juntion of Pipes,* Lappeenranta: Lappeenranta University of Technology.

Versteeg, H. & Malalasekera, W., 1995. *An Introduction to Computational Fluid Dynamics: The Finite Volume Method*. New York: Longman Scientific & Technical.

Wermac, 2008. *Explore the world of Piping: Definition and Details of Pipe*. [Online]
Available at: http://www.wermac.org/pipes/pipe_part1.html
[Accessed 3 May 2016].

WIKI2, 2015. *WIKI 2: Types of Mesh*. [Online]
Available at: https://en.wiki2.org/wiki/Types_of_mesh
[Accessed 24 April 2016].

Wikipedia, 2016. *Wikipedia*. [Online]
Available at: https://en.wikipedia.org/wiki/OpenFOAM
[Accessed 18 March 2016].

# Appendix A.

The convergence plot of blind-tee and elbow pipes case.
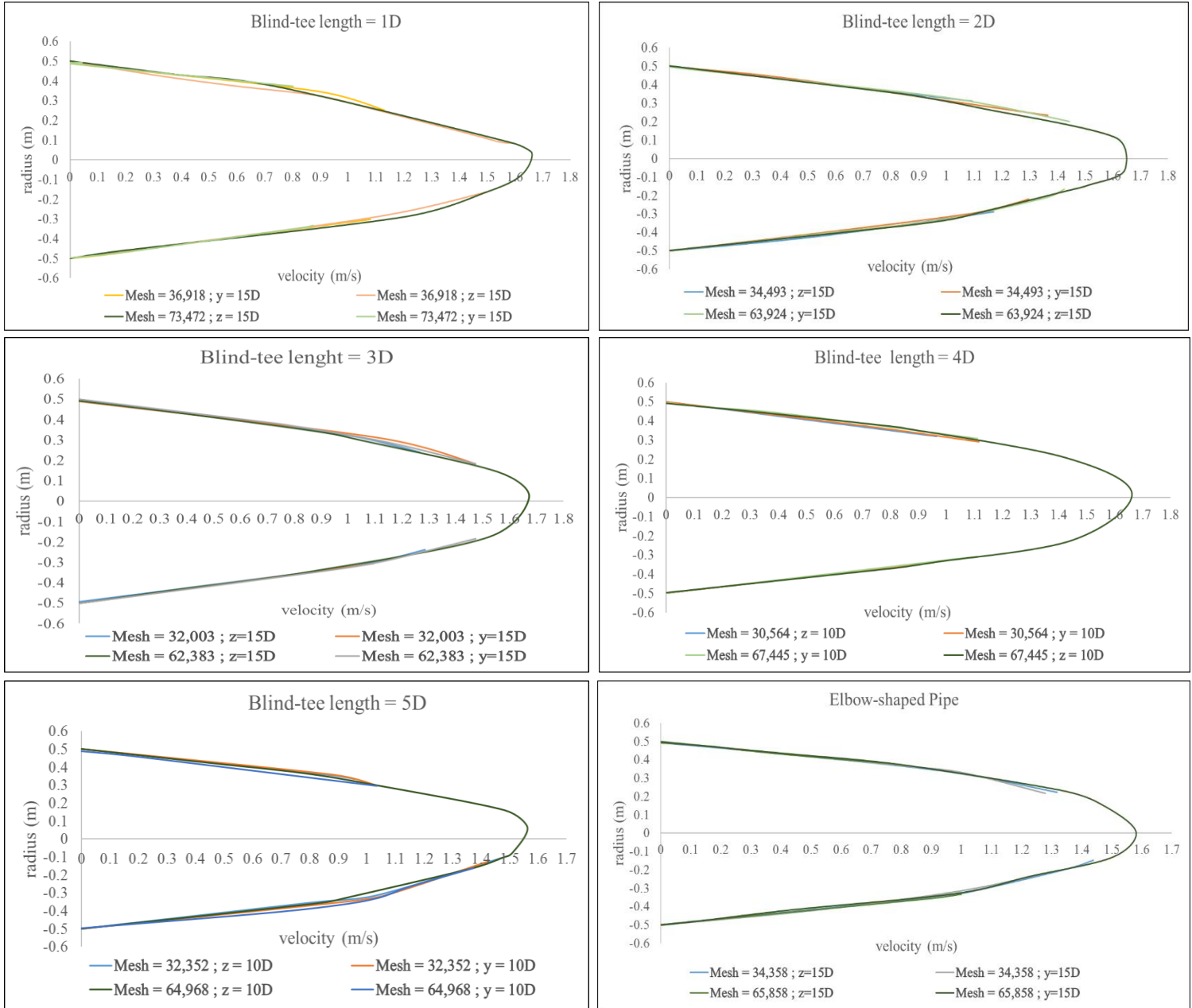
# Appendix B. Input File: 0

## B.1. Velocity (U)

```
FoamFile
{
   version   2.0;
   format    ascii;
   class     volVectorField;
   object    U;
}
// * * * * * * * * * * * * * * * * * * * * * * * * * * * * *
* * * * * * //

dimensions    [0 1 -1 0 0 0 0];
internalField  uniform (0 0 1);
boundaryField
{
   inlet
   {
     type        timeVaryingMappedFixedValue;
          setAverage     off;
     offset (0 0 0);
   }
   outlet
   {
     type        zeroGradient;
   }
   wall
   {
     type        fixedValue;
     value       uniform ( 0 0 0 );
   }
}
//
*************************************************
*********************** //
```

## B.2. Pressure (P)

```
FoamFile
{
   version   2.0;
   format    ascii;
   class     volScalarField;
   object    p;
}
// * * * * * * * * * * * * * * * * * * * * * * * * * * * * *
* * * * * * //

dimensions    [0 2 -2 0 0 0 0];
internalField  uniform 0;
boundaryField
{
   wall
   {
     type        zeroGradient;
   }
   inlet
   {
     type        zeroGradient;
   }
   outlet
   {
     type        fixedValue;
     value       uniform 0;
   }
}
//
*************************************************
*********************** //
```

66

# Appendix C. Input File: Constant

## C.1. Transport properties

```
FoamFile
{
    version    2.0;
    format     ascii;
    class      dictionary;
    location   "constant";
    object     transportProperties;
}
// * * * * * * * * * * * * * * * * * * * * * * * * * * * * * * * * * //
transportModel Newtonian;

nu            [0 2 -1 0 0 0 0] 1e-03;

//
*************************************************
************************* //
```

## C.2. Turbulence properties

```
FoamFile
{
    version    2.0;
    format     ascii;
    class      dictionary;
    location   "constant";
    object     turbulenceProperties;
}

// * * * * * * * * * * * * * * * * * * * * * * * * * * * * * * * * //

simulationType laminar;

*************************************************
*********************** //
```

# Appendix D. Input File: System

## D.1. controlDict

```
FoamFile
{
    version    2.0;
    format     ascii;
    class      dictionary;
    location   "system";
    object     controlDict;
}
// * * * * * * * * * * * * * * * * * * * * * * * * * * * * * * * * * * //

application    pimpleFoam;

startFrom      latestTime;

startTime      0;

stopAt         endTime;

endTime        400;

deltaT         0.01;

writeControl   adjustableRunTime;

writeInterval  10;

purgeWrite     0;

writeFormat    ascii;

writePrecision 6;

writeCompression off;

timeFormat     general;

timePrecision  6;

runTimeModifiable yes;

adjustTimeStep no;

//maxCo          0.3;
//maxDeltaT          1;

//
*************************************************
*********************** //
```

## D.2. fvSchemes

```
FoamFile
{
    version    2.0;
    format     ascii;
    class      dictionary;
    location   "system";
    object     fvSchemes;
}
// * * * * * * * * * * * * * * * * * * * * * * * * * * * * * * * * * * //
ddtSchemes
{
    default        Euler;
}
gradSchemes
{
    default        Gauss linear;
    grad(p)        Gauss linear;
    grad(U)        Gauss linear;
}
divSchemes
{
    default        none;
    div(phi,U)     bounded Gauss linearUpwind grad(U);
    div(phi,k)     bounded Gauss upwind;
    div(phi,epsilon) bounded Gauss upwind;
    div(phi,R)     bounded Gauss upwind;
    div(R)         Gauss linear;
    div(phi,nuTilda) bounded Gauss upwind;
    div((nuEff*dev2(T(grad(U))))) Gauss linear;
}
laplacianSchemes
{
    default        none;
    laplacian(nuEff,U) Gauss linear corrected;
    laplacian(rAUf,p) Gauss linear corrected;
    laplacian(DkEff,k) Gauss linear corrected;
    laplacian(DepsilonEff,epsilon) Gauss linear corrected;
    laplacian(DREff,R) Gauss linear corrected;
    laplacian(DnuTildaEff,nuTilda) Gauss linear corrected;
}
interpolationSchemes
{
    default        linear;
    interpolate(U) linear;
}
snGradSchemes
{
    default        corrected;
}
//
*************************************************
*********************** //
```

## D.3. fvSolutions

```
FoamFile
{
    version   2.0;
    format    ascii;
    class     dictionary;
    location  "system";
    object    fvSolution;
}
// * * * * * * * * * * * * * * * * * * * * * * * * * * * * *
* * * * * * //

solvers
{
    p
    {
        solver        GAMG;
        tolerance     1e-7;
        relTol        0.01;

        smoother      DICGaussSeidel;

        cacheAgglomeration  true;
        nCellsInCoarsestLevel 10;
        agglomerator      faceAreaPair;
        mergeLevels       1;
    }

    pFinal
    {
        $p;
        relTol        0;
    }

    "(U|k|epsilon)"
    {
        solver        smoothSolver;
        smoother      symGaussSeidel;
        tolerance     1e-05;
        relTol        0.1;
    }

    "(U|k|epsilon)Final"
    {
        $U;
        relTol        0;
    }
}

PIMPLE
{
    nNonOrthogonalCorrectors 0;
    nCorrectors        2;
}

//
*************************************************
*********************** //
```